

Contents:

- 8 Relationship of Thyroid Stimulating Hormone (TSH) levels and Bone Mineral Density (BMD) values among Overt Hyperthyroid Male patients in Jose R. Reyes Memorial Medical Center
Jayson U. Salibay, RMT, MD, Wenceslao Llauderres, MD, Marcelino Tanquilut, MD, Emelito Valdez-Tan, MD
- 16 Quantitative Ga-68 DOTATATE PET/CT Parameters for the Prediction of Response to Therapy in Patients with Well-Differentiated Neuroendocrine Tumors: A Correlational Study in a Tertiary Hospital in the Philippines
Lara Triccia C. Luistro, MD, Patrick Earl A. Fernando, MD, Chesterlee M. Ocampo, MD, Alfredo L. Marte II
- 26 OCCULT BREAST CANCER: A CASE REPORT
Belinda R. Dancel-San Juan, MD, MSc
- 30 F18-FDG PET-CT of Takayasu's Arteritis with Large Vessel Morphologic Changes in a Filipino Patient
Carlo Jose S. San Juan, MD
- 34 A Comparative Study of Two Commercial Software Programs in Measuring Myocardial Left Ventricular Perfusion and Function among Filipino Patients undergoing Gated SPECT-MPI
Mary Amie Gelina E. Dumatol, MD, Jerry M. Obaldo, MD, MHA, Apolonio Alecksandr T. Molina, RMT, MSMT

Connecting Every Step in Molecular Medicine



A Vision for Molecular Medicine.

DISCOVERY



for development of
targeted tracers
and therapy

DIAGNOSIS



with **breakthrough**
PET and SPECT
imaging solutions

TREATMENT



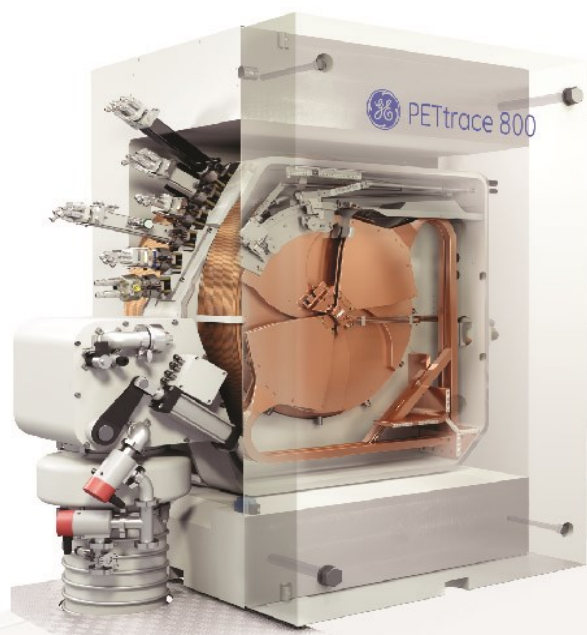
using **predictive**
and advanced
monitoring tools

We are focused on core challenges

At GE Healthcare we believe we can uniquely help connect the teams, data, and decisions in every step from discovery to diagnosis to treatment with intelligent efficient innovations that will ultimately help you deliver precise, personalized care. This is our vision.

There is so much data available across molecular imaging today. There are so many connection opportunities and loops to close. That's where we see significant opportunity. And we believe we're in a unique position to fulfill this vision because we are the only vendor with pharmaceutical diagnostics, cyclotrons, chemistry synthesis, PET/CT, SPECT/CT, advanced digital solutions and pharma partnerships to cover the breadth of steps from discovery to treatment.

Please contact your local GE Healthcare representative to learn more or visit <https://www.gehealthcare.com.sg/>



Philippine Journal of Nuclear Medicine

Volume 19 No. 2
July to December 2024

Official Publication of the Philippine Society of Nuclear Medicine

The Philippine Journal of Nuclear Medicine is a double blind peer-reviewed journal published by the Philippine Society of Nuclear Medicine. Subscription is free to all PSNM members in good standing as part of their membership privileges.

The Journal will be primarily of interest to medical and paramedical personnel working in nuclear medicine and related fields. Original works in clinical nuclear medicine and allied disciplines in physics, dosimetry, radiation biology, computer science, radiopharmacy, and radiochemistry are welcome. Review articles are usually solicited and published together with related reviews. Case reports of outstanding interest are likewise welcome. PSNM documents and position papers of interest to the reader will also be published as necessary.

Manuscripts for consideration should be sent to:

The Editor, Vincent Peter C. Magboo, MD
Philippine Journal of Nuclear Medicine
c/o Philippine Society of Nuclear Medicine
Unit 209 One Beatriz Tower Condo
4 Lauan St. cor. Aurora Blvd
Project 3, Quezon City 1102, Philippines
Contact. No.: +63 (966) 976 5676
Email: vcmagboo@up.edu.ph
philnucmed@gmail.com

All business communications and requests for complimentary copies should be addressed to the above.

Copyright©2024 by the Philippine Society of Nuclear Medicine, Inc. All rights reserved. No part of this work may be reproduced by electronic or

other means, or translated without written permission from the copyright owner. The copyright on articles published by the Philippine Journal of Nuclear Medicine is held by the PSNM, therefore, each author of accepted manuscripts must agree to automatic transfer of the copyright to the publishers. See Information for Authors for further instructions.

The copyright covers the exclusive rights to reproduce and distribute the articles. The publishers reserve the right to make available part or all of the contents of this work on the PSNM website (www.psnm.ph). Copyright of the contents of the website are likewise held by the PSNM.

ISSN 1655-9266

PSNM Publications Committee and PJNM Editorial Staff

Editor

Vincent Peter C. Magboo, MD

Associate Editors

Patricia A. Bautista-Penalosa, MD
Jeanelle Margareth T. Tang, MD

Editorial Board

Eric B. Cruz, MD
Michele A. Duldulao-Ogbac
Jonas Francisco Y. Santiago, MD
Asela B. Barroso, MD
Christopher Anthony G. Carbonell, MD
Johann Giovanni P. Mea, MD
Arnel E. Pauco, MD
Francis Gerard M. Estrada, MD

INFORMATION FOR AUTHORS

EDITORIAL POLICY

The Philippine Journal of Nuclear Medicine is the official double blind peer-reviewed publication of the Philippine Society of Nuclear Medicine. The Journal accepts original articles pertinent to the field of nuclear medicine. Articles may be on any of the following: clinical and basic sciences, case reports, technical notes, special contributions, and editorials.

Submission of manuscripts

The submitted manuscript package should consist of: (1) the full text (including tables) in Microsoft Word, plain text or ConTeXt document format; and (2) high-resolution JPEG files of all images used in the manuscript. The complete manuscript package may be submitted as a compressed (.ZIP) file by email to philnucmed@gmail.com, or in an optical disc (CD/DVD) and mailed to

The Editor: Philippine Journal of Nuclear Medicine, c/o Philippine Society of Nuclear Medicine, Unit 209 One Beatriz Tower Condo, 4 Luanan St. cor. Aurora Blvd., Project 3, Quezon City 1102, Philippines.

Manuscripts should be accompanied by a cover letter signed by the author responsible for correspondence regarding the manuscript. The cover letter should contain the following statement:

"All copyright ownership is transferred to the Philippine Journal of Nuclear Medicine upon acceptance of the article _____. This manuscript has been seen and approved by all the authors. The authors stipulate that the material submitted to the Philippine Journal of Nuclear Medicine is an original work and has not been submitted to another publication for concurrent consideration. Any human and/or animal studies undertaken as part of the research are in compliance with regulations of our institution(s) and with generally accepted guidelines governing such work."

The cover letter should also give any additional information that may be helpful to the Editor. Signed cover letters sent by email should be in PDF format.

MANUSCRIPT FORMAT

Manuscripts must be written in English, and printed on letter-sized white bond paper, 8.5 in x 11 in (21.6 cm x 27.9 cm). The text should be on one side of the

paper only, single-spaced, with at least 1.5 in (4 cm) margins on all sides. Each of the following sections must begin on separate pages and in the following order: title page, abstract, text, acknowledgments, references, tables (each on a separate page), and legends. Pages should be consecutively numbered beginning with the title page. The first line of paragraphs should be indented by at least five spaces.

Title page

The title page should include: (1) a concise but informative title; (2) a short running head or footline of no more than 40 characters; (3) a complete byline, with first name, middle initial, and last name of each author and highest academic degrees; (4) the complete affiliation for each author, with the name of departments and institutions to which the work should be attributed; (5) disclaimers, if any; (6) the name, address, and telephone number of the author responsible for correspondence about the manuscript; and (7) the name and address of author to whom reprint requests should be directed.

Abstract and key words

An abstract of no more than 300 words should state the purpose of the study or investigation, summary of methodology, major findings, and principal conclusions. New and important aspects of the study or observations should be emphasized. No figures, abbreviations or reference citations are to be used in the abstract.

Text

The text of original scientific and technical articles is usually divided into the following sections: Introduction, Materials and Methods, Results, Discussion, and Summary or Conclusion.

Case reports are divided into the following sections: Introduction, Case Report, Discussion, and Conclusion. They should contain a concise description of one to three patients, emphasizing the nuclear medicine aspects and include methodology, data and correlative studies. Procedures should be described in sufficient detail to allow other investigators to reproduce the results.

Other articles, e.g. review articles, position papers, or editorials, should introduce a problem or question, present evidence, and conclude with an answer. Generally, review articles should have extensive documentation. Literature citations should represent the breadth and depth of the subjects being reviewed. The organization of review articles will depend greatly on the subject matter and material.

Generic names must be used throughout the text. Instruments and radiopharmaceuticals must be identified by manufacturer name and address in parentheses.

Acknowledgments

Persons or agencies contributing substantially to the work, including any grant support, must be acknowledged.

References

References must be cited in consecutive numerical order at first mention in the text and designated by the reference number in parentheses. References appearing in a table or figure should be numbered sequentially with those in the text.

The reference list must be numbered consecutively as in the text. The journal follows Index Medicus style for references and abbreviates journal names according to the List of Journals Indexed in Index Medicus. 'Unpublished observations' and 'personal communications' should not be used as references, although written—not verbal—communications may be noted as such in the text. The author is responsible for the accuracy of all references and must verify them against the original document.

For journal articles with six or less authors, all authors must be listed. For those with seven or more authors, only the first three are listed, and "et al." is added to the end of the list.

Seabold JE, Conrad GR, Kimball DA, Ponto JA and Cricker JA. Pitfalls in establishing the diagnosis of deep venous thrombophlebitis by indium-111 platelet scintigraphy. *J Nucl Med* 1988;29:1169–1180.

For book and book chapters:

Williams LJ. Evaluation of parathyroid function. In: Brock LJ, Stein JB, eds. *The parathyroid and its diseases*. 4th ed. New York: Wiley; 1985:196–248.

Goodyear B. Bone marrow transplantation in severe combined immunodeficiency syndrome. In: Gree HJ, Blacksmith R, eds. *Proceedings of the fourth biennial meeting of the International Society of Transplantation*. Houston: International Society of Transplantation; 174: 44–46.

For journal article in electronic format:

Author. Title. Journal name. Online publishing date. Available from: URL address.

Tables

Each table should be typed double-spaced on a separate page. Do not submit tables as photographs. Tables should be self-explanatory and should supplement, not duplicate, the text. Each table must be cited in consecutive numerical order in the text. Tables should be numbered consecutively with a Roman number following the word TABLE.

Illustrations

Illustrations should clarify and augment the text. Figures should be sharp and of high quality. Glossy photographs of line drawings rendered professionally on white drawing paper in black India ink, with template or typeset lettering, should be submitted. High quality computer-generated art is also acceptable. Letters, numbers, and symbols should be clear and of sufficient size to retain legibility after reduction.

Each illustration must be numbered and cited in consecutive order in the text. Illustrations should be identified on a gummed label. Legends should be typed double-spaced on a separate page. Figures should be numbered with an Arabic number following the word FIGURE.

Units of measurement


Use of the International System of Units (SI) is standard. Measurements of length, height, weight, and volume must be reported in metric units. Other measurements must be reported in the units in which they were made. Alternative units (non-SI units) should be added in parentheses by the author, if indicated.

Abbreviations and symbols

Only standard abbreviations and symbols should be used in the text. At first mention, the complete term, followed by its abbreviations in parentheses, must be used in the text. Standard units of measure should not be expanded at first mention. Consult a style manual, if necessary.

REVIEW PROCEDURE

Submitted manuscripts are peer-reviewed for originality, significance, adequacy of documentation, reader interest, composition, and adherence to the guidelines. Manuscripts are returned to the author for revision if suggestions and criticisms have been made. All accepted manuscripts are subject to editing for scientific accuracy, clarity, and style.





An established global key
player in the **radioisotope**
& **radiopharmaceutical** field.

Find out more about
us and our products:



www.itm-radiopharma.com

Follow us:  

The logo consists of a small white dot above the letter 'i' in the word 'itm', which is rendered in a bold, lowercase, sans-serif font.

PASSION FOR PRECISION



MedChoice

**Thyroid &
Diabetes**

H E A L T H C A R E

Todo Aruga

Scan the QR code to know
more about our products.



MEDCHOICE ENDOCRINE GROUP INC.
Unit 901-1001, 88 Corporate Center
Sedeño corner Valero Street, Salcedo Village, Makati City
www.medchoicepharma.com

MTDH-03-012024

Relationship of Thyroid Stimulating Hormone (TSH) levels and Bone Mineral Density (BMD) values among Overt Hyperthyroid Male patients in Jose R. Reyes Memorial Medical Center

Jayson U. Salibay, RMT, MD, Wenceslao Llauderres, MD, Marcelino Tanquilut, MD,

Emelito Valdez-Tan, MD

Department of Nuclear Medicine, Jose R. Reyes Memorial Medical Center

E-mail address: mejus2007@gmail.com

ABSTRACT

Introduction:

Hyperthyroidism is defined as a thyrotoxicosis resulting from a hyper-functioning thyroid gland tissue. In state of hyperthyroidism, complication onset warrants prompt clinical control to subdue morbidity and mortality outcomes. There are no studies made so far on the relationship and effect of hyperthyroidism on bone mineral density outcome among young male patients with overt thyroid disease.

Objectives:

(a) to determine the relationship of average baseline TSH level and BMD value measured by Dual Energy X-ray Absorptiometry (DEXA) scan to average TSH and BMD value after 1 year of treatment; (b) to determine the relationship of average TSH result to middle radio-ulna (MRU), lumbar spine (LS) and femoral neck (FN) sites BMD values after 1 year of treatment and; (c) to describe overt hyperthyroid male patients as to incidence of low BMD that might suggest osteoporosis among TSH results.

Methodology:

A longitudinal, prospective cohort study design was applied with BMD measurements before and after treatment among male patient age 20-45 years with newly diagnosed overt hyperthyroid disease. DEXA was utilized to measure MRU, LS and FN sites before and after 1 year of treatment. Patient's clinical data was recorded. Pearson product moment correlation analysis was utilized to determine the first and second objectives. Mean and standard deviation were used to present continuous variables while categorical data were presented by frequency and percentage. Statistical product service solution version 24 was used to carry out statistical calculations. The level of significance was set at 95% confidence or < 0.05 .

Results:

A total of 14 eligible patients volunteered for the study with mean age of 31.07 ± 6.62 years. Only 4 subjects completed the course. Six subjects were interrupted by COVID-19 pandemic, 3 subjects dropped and 1 subject died along the course. The cause of death is related to the natural process of the disease. Ninety-three percent of subjects used Methimazole while 7% used Propylthiouracil as anti-thyroid drug. Results shows that mean baseline TSH and BMD values for MRU and LS sites are not significantly related to mean TSH and mean BMD values of 3 sites after 1 year of treatment ($p > 0.05$). Mean baseline MRU is significantly related to mean FN BMD post 1 year with strong correlation, p value of 0.043 and $r = 0.957$. Mean TSH and mean BMD values for MRU, LS and FN sites after 1 year of treatment shows no significant relationship ($p > 0.05$). Due to lack of number of cases who completed the study due to COVID-19 pandemic, further analysis for objective 3 could not be performed.

Conclusion:

This study is inconclusive with regards to TSH level in relation to BMD outcome among overt hyperthyroid male patient age 20 – 45 years due to sample size limitation.

Keywords: bone mineral density, TSH, young male, hyperthyroidism, Filipino

INTRODUCTION

Hyperthyroidism is defined as a thyrotoxicosis, high level of circulating thyroid hormone, resulting from a hyperfunctioning thyroid gland tissue [1]. In National Health and Nutrition Examination Survey III (NHANES III) Study, 'clinically significant' (overt) hyperthyroidism is defined as a serum TSH concentration <0.1 mIU/L and a serum Total T4 concentration >170 nmol/L [2]. In hyperthyroidism, females are the most commonly affected gender in comparison to males with 4:1 ratio; so with the frequency of thyroid nodules among aging (> 60 y.o.) population, 6.4% of women and 1.5% of men [3]. Peak age-specific incidence of Graves' disease varies among different ethnic backgrounds [4].

In state of hyperthyroidism, complication onset warrants prompt clinical control to subdue morbidity and mortality outcomes. In one observational cohort study comparing mortality outcomes of treated versus non-treated hyperthyroidism patients, there was an excess of mortality in the individuals who did not receive anti-thyroid treatment as compared with euthyroid controls [5]. Complications or outcomes of overt hyperthyroidism are cognitive dysfunction in acute phase [6], high heart failure risk [7], hypokalemic paralysis [8], low bone mineral density [9] and rare outcomes such as thyroid storm and cerebral venous thrombosis [10]. Detrimental effect on bones as a complication of overt hyperthyroidism was first documented in 1891 [11]. This has been so far the traditional view of direct effect of thyroid hormone elevation on bone mineralization. However, recent studies cited relationship of bone resorption to low TSH levels as an independent factor [12] with findings that treatment or normalization of TSH levels has anti-resorptive effect [11].

There are no studies made on the relationship and effect of hyperthyroidism on bone mineral density outcome among young male patients with overt disease.

OBJECTIVES

The aims of this study are: (a) to determine the relationship of average baseline TSH level and BMD value measured by DEXA scan to average TSH value and BMD result after 1 year of treatment; (b) to determine the relationship of average TSH results to MRU site, LS site and FN site BMD values generated by DEXA scan after 1 year of treatment and; (c) to describe overt hyperthyroid male patients age 20-45 years old as to incidence of low BMD that might suggest osteoporosis among TSH results

after 1 year of treatment.

LIMITATION OF THE STUDY

This study is limited only in observing the effect of TSH to bone BMD levels. Factors such as physical activity, alcohol, cigarette smoking, diet, medications taken aside from drugs related to the disease under investigation and anti-thyroid drugs are not evaluated during the course of this research .

METHODOLOGY

Study Design

A longitudinal, prospective cohort research design was used in this study. The research period was conducted between the months of August 2018 to August 2019. Sample population is taken using purposive sampling method based on objectives of this study and characteristics such as newly diagnosed overt hyperthyroid case, male patient age 20-45 years, seen and referred to the Department of Nuclear Medicine of Jose R. Reyes Memorial Medical Center and patients who decided not to or declined RAI recommendation for overt hyperthyroidism treatment due to any reasons reserve by the patient.

Patients diagnosed with asthma, COPD, neoplastic diseases, endocrine diseases not thyroid-related, those who received RAI therapy, autoimmune disease, renal disease, epilepsy and primary bone diseases were excluded. Patients who are current smoker, unable to provide written consent, unlikely to undergo DEXA scan and follow-up, taking immunosuppressive drugs, and glucocorticoid and anticonvulsant drugs; and those with history of heavy alcohol use were likewise excluded. The study protocol was reviewed and approved by Institutional Review Board of this institution.

From the start of the study; FT4 and TSH obtained via radioimmunoassay, thyroid scan and neck ultrasound, all done at our institution, were collated. Baseline DEXA scan was requested. Patient data such as age, height and weight in relation to body mass index, type of medications used (both anti-thyroid drugs and non-thyroid related medications) prescribed by their respective physicians, drug dosage, time span of treatment, smoking history, alcoholic beverage consumption, history of fracture, family history of thyroid disease and osteoporosis, FT4 and TSH results were recorded and collected every after 2 months. Patients were followed up for 1 year .

Dual Energy X-Ray Absorptiometry (DEXA) Protocol

In DEXA scan measures BMD of MRU, LS and FN (either side) as regions of interest. Values of BMD at lumbar spine will be calculated as a mean of L1-L4 vertebra and images are obtained in postero-anterior acquisition. In cases of large value differences between each lumbar vertebra, a standard deviation beyond 1 of a particular vertebra will be excluded in the computation. Thirty-three percent of the total length of the non-dominant radio-ulna region will be image and BMD value will be generated out from it. Femoral neck region measurement could be taken on either sides of the hip.

To avoid discrepancies in BMD results a single DEXA machine will be used, HOLOGIC Wi Discovery Bone Densitometer®, and same operator will measure all subjects. DEXA scan results will be read by at least two (2) certified Nuclear Medicine specialist of the Department. The interpretations for results are consensus made by these physicians. The interpretations are in accordance with the existing guidelines of the International Society for Clinical Densitometry.

Statistical Analysis

The Pearson Product Moment Correlation analysis was utilized to determine the first and second objectives. Descriptive statistics such as mean and standard deviation were used to present continuous variables such as age, FT4, TSH, BMD and BMI. While categorical data such as chief complaint, drug type, fracture history and family clinical history were presented by frequency and percentage. Statistical Product Service Solution version 24 was used to carry out statistical calculations with level of significance set at 95% confidence or < 0.05.

RESULTS

A total of 14 subjects were enrolled in the study, the mean age of the patient was 31.07±6.62. Out of 14, only 4 subjects completed the 1 year follow-up, 6 subjects were interrupted by COVID-19 pandemic during the course, 3 subjects dropped and 1 subject died during the course. The cause of death is related to the natural process of the disease. Ninety-three percent (13) of subjects used Methimazole while 7% (1) used Propylthiouracil as anti-thyroid drug.

TABLE 1. Demographic and Clinical Profile

Variable	Values
Age	31.07 ± 6.62
Chief Complaint	
Palpitation	5 (36 %)
Weight Loss	4 (29 %)
Lower Extremity Weakness	2 (14 %)
Anterior neck mass	2 (14 %)
Tremors at rest	1 (7 %)
SPY	3.51 ± 4.24
MaxA (Liter) per visit	0.25 ± 0.29
ATD	
M	13 (93 %)
PTU	1 (7 %)
Total D1 (g) per visit OD	1.11 ± 0.59
Total D2 (g) per visit	0.18 ± 0.21
Total D3 (g) per visit	98.72 ± 162.05
Total D4 (g) per visit	0.57 ± 0.21
BMI (kg/m ²)	12.47 ± 5.13
FRX	
Y	2 (14 %)
N	12 (86 %)
FHX	
Y	7 (50 %)
N	7 (50 %)
FT4	38.86 ± 4.57
TSH	17.05 ± 7.91
BMI	7.91 ± 3.19
Legend: SPY (smoking pack years), MaxA (maximum alcohol volume intake), ATD (anti-thyroid drug), M (Methimazole), PTU (Propylthiouracil), OD (other drugs), BMI (body mass index), Frx (history of fracture), FHx (family history of thyroid disease and osteoporosis), TSH (thyroid stimulating hormone), Y (yes) and N (no)	

Table 2 shows the Pearson Product Moment Correlation analysis between the mean baseline TSH and BMD and mean TSH and BMD post 1 year result. It shows that in terms of TSH mean, none from the baseline TSH, MRU, LS and FN showed statistically significant correlation (p -value > 0.05). In terms of the MRU post 1 year, none also showed statistical relationship in any of the baseline TSH, MRU, LS and FN. For LS, the same results were also observed where none showed statistical correlation between the same parameters. However, for FN post 1 year, only MRU showed an $r = 0.957$ with a p -value of 0.043. This means that FN post 1 year values has a significantly strong correlation with MRU values at baseline. Furthermore, 91% in the total variations in FN post 1 year can be explained by MRU.

TABLE 2. Correlation table for mean baseline TSH and BMD values versus mean TSH and BMD values after 1 year of treatment

Mean Post 1 Year		Mean Baseline			
		TSH	MRU	LS	FN
TSH	r	-0.068	0.102	-0.143	0.138
	p-value	0.816	0.728	0.627	0.637
MRU	r	0.322	0.888	-0.507	0.842
	p-value	0.678	0.112	0.493	0.158
LS	r	0.919	0.091	0.621	0.724
	p-value	0.081	0.909	0.379	0.276
FN	r	0.258	0.957	-0.569	0.726
	p-value	0.742	0.043	0.431	0.274

Correlation to baseline TSH level and BMD value to mean TSH value and BMD result after 1 year of treatment, only baseline MRU showed significantly strong correlation with FN post 1 year value ($r = 0.957$; p -value < 0.05). Legend: Thyroid stimulating hormone (TSH), middle radio-ulna (MRU), lumbar spine (LS) and femoral neck (FN)

Table 3 shows the Pearson Product Moment Correlation Analysis between the mean TSH and mean BMD post 1 year result. It shows that in terms of MRU, LS and FN, no significant statistical relationship was found among the parameters

TABLE 3. Correlation table for mean TSH and BMD values after 1 year

Mean Post 1 Year	Mean TSH	
	TSH	MRU
MRU	r	0.587
	p-value	0.413
LS	r	-0.562
	p-value	0.438
FN	r	0.709
	p-value	0.291

Legend: Thyroid stimulating hormone (TSH), middle radio-ulna (MRU), lumbar spine (LS) and femoral neck (FN)

Due to lack of number of cases who completed the study due to COVID-19 pandemic, further analysis for objective number 3 could not be performed.

DISCUSSION

The traditional view on the direct effect of thyroid hormone elevation on bone mineralization was challenged by molecular studies of Abe et al [13] and Baliram et al [14]; and clinical studies of Svare et al [11], Jodar et al [15] and Chin et al [16] that TSH level independently played a significant role in skeletal integrity. This is clinically apparent when observing the BMD outcome of various skeletal sites among subclinical hyperthyroid patients [17], but there are no studies made on the relationship of overt hyperthyroidism to bone mineral density outcome especially among young male patients. The results of this study shows that there is no significant correlation between mean baselines and mean TSH post 1 year to post 1 year BMD parameter values of MRU, LS and FN (Table 2 & 3). Further, this study shows that there is a direct correlation of post 1 year FN BMD with baseline MRU BMD, (strong $r = 0.957$; p -value < 0.05), but no correlation to LS site post 1 year (p -value > 0.05) (Table 2). No statistical significance showed in baseline and post 1 year MRU BMD values. As observed, the association of mean TSH to baseline TSH and MRU site post 1 year did not reached significance, p -value > 0.05 . Observations made by those previous

studies are somehow similar in clinical question using different tools for BMD measurement .

In Svare et al [11] study, about 6,722 women age ≥ 40 years who underwent BMD measurement (using single-energy densitometers) with TSH correlation showed decrease distal forearm BMD (10.7 mg/cm²) in relation to low TSH level (TSH <0.5 mU/L). The study only have 3.2% cases with current hyperthyroidism (n = 215) of which 8.1% with medical treatment (n ~ 18). In the study of Chin et al [16], about 681 Chinese and Malay male patients with mean age 48.5 years were screened using calcaneal speed of sound (SOS) measurement against TSH levels without apparent clinical thyroid disease. A multiple regression analysis revealed that TSH was significantly and positively associated with calcaneal SOS after adjustment for age (p-value < 0.05) computed. In Jodar et al study [15], 32 Spanish male patients with recent onset of Graves' disease under Carbimazole (TSH 1.07 ± 1.8 μ U/mL and mean age 43 ± 12) were studied by measuring lumbar (L2-L4), femoral neck and ward's triangle (WT) BMD using DEXA. After excluding those with elevated FT4 levels, the significant reduction of BMD was maintained in LS and FN (-0.71 ± 0.94 and -0.49 ± 0.48 , respectively), but not in WT BMD (-0.31 ± 1.13). These studies showed that TSH level and BMD value are correlated to each other. A decrease in TSH level results to a decrease in BMD value. The result of our study disputes this claim.

Bone metabolism in hyperthyroidism is characterized by increase in both osteoclastic and osteoblastic activities, especially in cortical bone [18]. This observation was not clinically observable because of differences of bone turnover rate between various bone compositions from various skeletal sites [19], 3%/year for cortical bone and 30%/year for trabecular bone. A classical study by Seeman et al [19], revealed the differences on the effect of hyperthyroidism to axial and appendicular skeletal BMDs among 13 subjects (n = 11 females, 2 males) with mean disease duration of 13 months. Mean age was not declared in the said study. The result of the said study revealed a positive deviation from normal age-specific and sex-specific mean BMD using Two-tail p value analysis associated with paired t test of mean BMD difference for two sites, -0.70 and -0.82 respectively for middle radius and lumbar spine. The study also showed approximate site bone composition, $>95\%$ cortical bone and $>66\%$ trabecular bone respectively. This means that appendicular bones are more readily affected than axial bones in overt state of hyperthyroidism. It shows that the appendicular skeleton like mid radio-ulna and femur, are more readily affected in overt hyperthyroidism in

terms of BMD outcome. This finding is also supported with the result of our study between correlations of baseline MRU to FN BMD post 1 year and baseline MRU to LS BMD post 1 year (Table 2). Compared to Seeman et al [19], in his study there was only a marginal decrease of appendicular skeletal BMD. Age in some extent also is protective from bone loss during thyrotoxicosis as shown by Fraser et al study [20], but our study shows that among male patients age 20–45 years their appendicular BMD changed along the course of the disease.

The significance of this study lies on challenging the contesting evidences of TSH as an independent factor affecting BMD outcome in hyperthyroidism. The result shows a different data about BMD measured using DEXA. No similar data on overt hyperthyroidism especially among young male population were ever documented so far.

CONCLUSION

This study is inconclusive with regards to TSH level in relation to BMD outcome among overt hyperthyroid male patient age 20 – 45 years due to sample size limitation.

RECOMMENDATION

This study was limited by the number of subjects thus more samples are needed for research continuation.

REFERENCES

1. Ziessman, H. et al., Nuclear Medicine: The Requisite. 4th Edition. 2014. Part II Clinical Nuclear Medicine Endocrine System. Chapter 6; 74.
2. Hollowell, JG. et al., Serum TSH, T4 and Thyroid antibodies in the United States population (1988 – 1994): National Health and Nutrition Examination Survey (NHANES III). Journal on Clinical Endocrinology and Metabolism. 2002; 87: 489 – 499.
3. Vanderpump, M. et al., The epidemiology of thyroid disease. British Medical Bulletin. 2011. 99: 39 – 51
4. Zimmerman, MB. et al., Iodine deficiency. Endocrinology Review. 2009. 30: 376 - 408.
5. Lillevang – Johansen, M. et al., Excess mortality in Treated and Untreated Hyperthyroidism is related to cumulative periods of low serum TSH. Journal of Clinical Endocrinology & Metabolism. July 1, 2017. Vol. 102, Issue 7: 2301 – 2309.
6. Vogel et al., Affective symptoms and cognitive functions in the acute phase of Grave's thyrotoxicosis.

- Psychoneuroendocrinology. 2007. Jan; 32(1): 36 – 43
7. Biondi, B. et al., Mechanisms in Endocrinology: heart failure and thyroid dysfunction. *European Journal of Endocrinology*. 2012. Nov. 167(5): 609 – 618.
 8. Salih, M. et al., Thyrotoxic periodic paralysis: an unusual presentation of hyperthyroidism. *The Netherlands Journal of Medicine*. October 2017. Vol. 75. No. 8: 315 – 320.
 9. Vestergaard, P. et al., Hyperthyroidism, bone mineral and fracture risk – a metaanalysis. *Thyroid*. 2003 June; 13(6): 585 – 593.
 10. Verbeme, HJ. et al., Thyrotoxicosis as a predisposing factor for cerebral venous thrombosis. *Thyroid*. 2000 July 10(7): 607 – 610.
 11. Svare, A. et al., Hyperthyroidism levels of TSH correlate with low bone mineral density: the HUNT 2 study. *European Journal of Endocrinology* (2009). 161:779 – 786.
 12. Galliford et al., Effects of thyroid status on bone metabolism: a primary role for thyroid stimulating hormone or thyroid hormone? *Minerva Endocrinologica* 2005(30): 237 – 246.
 13. Abe, E. et al., TSH is a negative regulator of Skeletal remodeling. *Cell*, Vol. 115. 2003. 151 – 162.
 14. Baliram, R. et al., Hyperthyroid-associated osteoporosis is exacerbated by the loss of TSH signaling. *The Journal of Clinical Investigation*. Vol. 122. No. 10. October 2012.
 15. Jódar, E. et al., Bone mineral density in male patients with L-thyroxine suppressive therapy and Grave's disease. *Calcif. Tissue Int*. 2001 August, 69(2): 84 – 87.
 16. Chin, K. et al., Thyroid-stimulating Hormone is Significantly Associated with Bone Health Status in Men. *International Journal of Medical Sciences*. 2013; 10(7): 857 – 863
 17. Kim, T. et al., A Modest Protective Effect on Thyrotropin against Bone Loss is Associated with Plasma Triiodothyronine levels. *PLoS One* 10(12): e0145292. doi. 10.1371/journal.pone.0145292 (2015).
 18. Mosekilde, L. et al., Bone changes in hyperthyroidism: Interrelationship between bone morphometry, thyroid function and calcium-phosphorus metabolism. *Acta Endocrinol (Copenh)*. 85:515 – 525.
 19. Seeman, E. et al., Differential Effects of Endocrine Dysfunction on the Axial and the appendicular skeleton. *The Journal of Clinical Investigation*. 1982; 69(6): 1302 – 1309.
 20. Fraser, S. et al., Osteoporosis and fractures following thyrotoxicosis. *Lancet*. 1971. I: 981 – 983.

transmedic

LEADING MEDICAL EQUIPMENT SPECIALIST IN SOUTHEAST ASIA

ABOUT US ...

TRANSMEDIC PHILIPPINES, INC. currently serves the needs of some of the country's top hospitals and medical clinics for - *external beam radiation therapy and also radiation therapy planning system, radiofrequency ablation systems & clinical support, vascular imaging requirements, LDR brachytherapy requirements, laparoscopy towers, beds, and other advanced medical technologies.* All in all, the Company has stood for the introduction of new technology for use in the local medical market to improve patient care & services, and/or to optimize cost efficiency.

LEARN MORE ...

+632 53176888

info.ph@transmedicgroup.com

<http://www.transmedicgroup.com/>



Best [®] **ABT** *Molecular Imaging*



mim **SurePlan**.MRT



SurePlan.LiverY90

Taking the Lead in PET/CT Imaging and Innovative Radiopharmaceuticals

OUR MANAGED PET/CT CENTERS

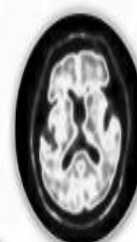


[18F]-FDG




A sugar analog used to detect metabolically active malignant lesions. A non-invasive approach to accurate diagnosis and staging for the optimal management of cancer patients

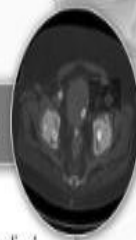
[18F]-FBB



Developed for routine clinical application to visualize beta amyloid neuritic plaque density. An effective tool to differentiate Alzheimer's Disease from other forms of Dementia

Khealth: The only licensed manufacturer of 

[18F]-FPSMA



Named as a top medical innovation by Cleveland Clinic in 2022. PSMA PET scan has greater sensitivity and can detect prostate cancer metastases sooner, allowing clinicians to better serve patients and make treatment decisions

[177Lu]-LUPPSMA



Partnered with PSMA-directed PETCT scan, LuPSMA offers a Theranostic approach to treatment of metastatic castration-resistant prostate cancer (mCRPC)

FOR PET/CT FINANCIAL ASSISTANCE:



**PET/CT
PATIENT
SUPPORT**

+63 998 323 5425
+63 917 714 4248
+63 917 714 4266
patientsupport@khealthcorp.com

Quantitative Ga-68 DOTATATE PET/CT Parameters for the Prediction of Response to Therapy in Patients with Well-Differentiated Neuroendocrine Tumors: A Correlational Study in a Tertiary Hospital in the Philippines

Lara Triccia C. Luistro, MD¹, Patrick Earl A. Fernando, MD¹, Chesterlee M. Ocampo, MD², Alfredo L. Marte II²

¹Department of Nuclear Medicine and Theranostics, St. Luke's Medical Center—Global City

²Institute of Radiology, St. Luke's Medical Center - Global City

E-mail address: triccia_02@ymail.com

ABSTRACT

Objective:

The goal of our study is to determine if Ga-68 DOTATATE PET/CT parameters can predict tumoral response to therapy by establishing good correlation with RECIST 1.1.

Methodology:

Review of the pre- and post-treatment Ga-68 DOTATATE PET/CT scans of 19 patients diagnosed with neuroendocrine tumors to acquire SUVmax, tumor SUVav, total lesion activity, molecular tumor volume, tumor-to-spleen and tumor-to-liver ratios, and tumor size and correlate the results with RECIST 1.1 to determine if patients are responders or non-responders.

Results:

Baseline molecular tumor volume and total lesion activity can discriminate between responders and non-responders. Using a threshold of 37.76 cm³ for molecular tumor volume and 60.95 SUV • cm³ for total lesion activity, response to treatment is predicted with a sensitivity of 100% and specificity of 53.8% and 66.7% and 92.3%, respectively, with area under the curve of 0.78 (95% CI 0.56 to 1.0) and 0.81 (95% CI 0.58 to 1.0), respectively.

Conclusion:

Ga-68 DOTATATE PET/CT scans may be used not only in staging of disease but also in predicting response to treatment. The total lesion activity has acceptable sensitivity and specificity to classify patients as responders or non-responders. This can provide clinicians an additional parameter for treatment response evaluation in neuroendocrine tumors.

Keywords: DOTATATE, PRRT, total lesion activity, metabolic tumor volume

INTRODUCTION

Neuroendocrine neoplasms show dense core granules similar to neuronal cells which contains the monoamine hormones [1]. They are either functioning or non-functioning, clinically characterized as to whether they present with symptoms of hormone overproduction [2]. They are categorized histologically by the 2022 WHO Classification of Endocrine and Neuroendocrine Tumors as well-differentiated neuroendocrine tumors (NETs) and poorly differentiated neuroendocrine carcinomas (NECs) [3]. The former is subdivided into Grades 1, 2 and 3 based on histologic proliferation parameters such as Ki-67 and number of mitotic figures. Most neuroendocrine neoplasms arise from the gastrointestinal tract and lungs [4, 5]. G1 tumors of the gastrointestinal tract and pancreas have < 2 mitotic figures per 2 mm² with Ki-67 proliferation index of < 3%, G2 has 2-20 mitotic figures per per 2 mm² and Ki-67 of 3 - 20% while G3 tumors have 20 mitotic figures per 2 mm² and Ki-67 index of > 20%. G1 tumors of the lungs and salivary glands have es/2 mm² and no necrosis, and Ki67 < 20%, G2 has 2 to10 mitoses per 2 mm² and/or necrosis, and Ki67 < 20% and G has > 10 mitoses/2 mm² and/or Ki67 > 20%. Staging is based on the American Joint Committee on Cancer (AJCC) 8th Edition Staging System. NETs can be considered as either early stage (completely resectable) or advanced stage (either locally advanced and unresectable or metastatic) [6].

Diagnostic imaging modalities for NETs and NECs include standard cross-sectional imaging with computed tomography (CT) and magnetic resonance imaging (MRI). Functional imaging takes advantage of the overexpression of somatostatin receptors in these tumors. The first scintigraphic imaging of neuroendocrine neoplasms was done in 1989 using radioiodinated tyr-3-octreotide. Indium-111 labelled radioactive tracers then became widely used to detect NENs for planar, single photon emission computed tomography (SPECT) and SPECT/CT imaging [7]. The inherent low resolution of the gamma camera limits the detection of small lesions and those with a small amount of somatostatin receptors. This disadvantage has been overcome by the advent of new radiotracers for positron emission tomography (PET) with octreotide-like properties. The three Ga-68 peptides available are DOTATATE, DOTANOC and DOTATOC. Improved detection leads to more aggressive management of lesions undetected by both CT and SPECT especially for bone metastases [8]. A comparison of Ga-68 DOTATATE and In-111 pentetreotide. The specificity of Ga-68

DOTATATE and In-111 pentetreotide are comparable but the sensitivity of DOTATATE PET imaging (96%; 95% CI, 86%–100%) is higher [9]. The normal biodistribution of DOTA-peptide tracers in the liver limits optimal evaluation of hepatic lesions but combining PET with CT shows higher accuracy for these lesions.

Treatment of NETs require complete surgical resection to be performed whenever possible for curative intent [10]. Medical management including somatostatin analogs, peptide receptor radionuclide therapy (PRRT), interferon -alpha, mTOR and VEGF inhibitors, and chemotherapy amongst others are given to control symptoms caused by excessive hormone production, and to control tumor growth and spread [11].

Theranostics, a term to denote combined diagnostics and therapy, uses the same ligand to diagnose and subsequently treat a tumor. It has only been recently available in the country through the efforts of PA Bautista in 2017. A prerequisite for doing therapy with the same ligand is to establish its uptake during diagnostic PET imaging. Imaging is performed in St. Luke's Medical Center using Ga-68 DOTATATE for NETs and Ga-68 prostate specific membrane antigen (PSMA) for prostate carcinoma. PRRT in the country is performed using Lu-177 DOTATATE. The first PRRT was successfully performed in the country on May 16, 2018 [12] and so far the results of the patient currently undergoing treatment have been promising. As of this writing, St. Luke's Medical Center is the only institution capable of DOTATATE PET imaging.

The best assessment tool to determine treatment response specifically of neuroendocrine tumors has not been well-established. The objective criteria to evaluate response to treatment in malignancies is the Response Evaluation Criteria in Solid Tumors (RECIST) 1.1. A complete response is resolution of all measurable lesions while partial response is reduction by > 30% in sum of all target lesions in longest axis measurement. Progressive disease is an increase by > 20%. Stable disease means not meeting the criteria for either progressive disease or partial response. For PET imaging, a positron emission tomography response criteria (PERCIST) in solid tumors has been developed exclusively for F-18 FDG PET, measuring the highest tumoral uptake (SUVmax) corrected to the lean body mass (SUV peak). Complete metabolic response is reduction of FDG uptake by all lesions to that below the background blood pool activity. Partial metabolic response means a decrease by at least 30% with at least a 0.8 unit decline in the SUV peak of the hottest lesion together with < 30% increase

in the SUV of the rest of the lesions with no new FDG-avid lesions. Progressive metabolic disease is an increase of at least 30% and 0.8 unit of the SUL peak or more than 75% increase in the total lesion glycolysis value or new FDG-avid lesions [13]. A PERCIST-like treatment response criteria for NETs has not been developed yet.

Several studies have tried to analyze the correlation between DOTATATE PET SUV parameters like baseline tumoral maximum DOTATATE uptake (maximum standard uptake value, SUVmax), the ratio of tumoral maximum DOTATATE uptake versus mean liver uptake (tumor-to-liver SUV ratio), tumor-to-spleen SUV ratio, and SUV max average (SUV max combined from at least 5 lesions) and treatment response, progression-free survival and overall survival [14 - 17]. SUVmax measured on Ga- 68 DOTANOC PET/CT is an independent positive prognostic factor in patients with well-differentiated NET and is superior to SUVmax on F18-FDG PET/CT [17]. Lee et al in 2021 reported that SUVmax on Ga-68 DOTATATE PET can predict therapeutic failure with sensitivity and specificity of 39% and 98%, respectively with an SUVmax of < 18.35 predicting short progression free survival. Campana et al in 2010 reported differentiation between patients with stable disease (SD) or a partial response (PR) at follow-up and patients with progressive disease (PD) ranged from 17.6 to 19.3. Sharma et al in 2019 reported a single lesion DOTATATE PET SUVmax cut-off of 13.0 to predict response to PRRT, giving a sensitivity and specificity of 0.83 (95% CI: 0.36–1.0) and 0.84 (95% CI: 0.67–0.95) ($p = 0.031$), respectively with an SUV max-average cut off of 10.2 the sensitivity and specificity in prognosticating a favorable treatment response was 0.80 (95% CI 0.67–0.96) and 0.83 (95% CI 0.45–1.15), respectively. For Ga-68 DOTATOC PET, Kratochwil et al in 2014 proposed a SUV max cut-off of 16.4 on to predict responding lesions to PRRT while for Oksuz et al in 2013, SUV max cut-off is 17.9. Another study has reported a DOTATOC SUV max of 13.7 cut-off to predict overall survival [18] .

OBJECTIVES

General Objective

To predict response to therapy of well-differentiated neuroendocrine tumors using baseline Ga-68 DOTATATE PET quantitative parameters

Specific Objectives

To compare RECIST 1.1 partial response, complete response, stable disease, progressive disease to change

in quantitative SUV parameters (SUV max, tumor-to-liver and tumor-to-spleen SUV ratios, and SUV max average) in predicting treatment response.

To determine a quantitative threshold (i.e. SUVmax cut-off) which can predict treatment response.

To describe whether change in the quantitative SUV parameters differs between treatment modalities (ex. chemotherapy, Lutetium-177 DOTATATE).

Significance of the Study

This study will help patients diagnosed with NETs on the expected benefit of somatostatin analog therapy or PRRT for well-differentiated neuroendocrine tumors. Research on NETs in the Philippines is lacking, admittedly due to the sheer infrequency of the disease relative to other malignancies, unfortunately leading to high cost of care. A study on disease prognostication through imaging will be adjunctive to both proper patient care and judicious allocation of patient resources in the management of the disease. The cost of targeted therapy for neuroendocrine tumor is high in the country thus predicting response can help in the decision-making of patients and their physicians.

METHODOLOGY

We conducted an IERC-approved retrospective analysis of patients who have biopsy-proven well-differentiated neuroendocrine tumors and who underwent at least two Ga-68 DOTATATE PET/CT scans.

Criteria for Subject Selection

Inclusion Criteria

Adult patients diagnosed with well-differentiated NETs (Grades 1 to 3) who underwent at least two DOTATATE PET/CT scans with treatment in between whether chemotherapy, immunotherapy, SSA analogues or PRRT from 2018 to September 9, 2023.

Exclusion Criteria

Patients who had F-18 fluorodeoxyglucose PET scan as a baseline scan prior to treatment and with a DOTATATE PET scan as follow-up.

Patients who had complete surgical resection of the primary tumor in between the DOTATATE scans.

Patients with lesions only measurable on CT scan alone or PET scan alone.

Operational Definitions

Fluorine-18 Fluorodeoxyglucose (F-18 FDG) – A glucose analog positron-emitting radionuclide.

Gallium-68 tetraazacyclododecanetetraacetic acid-DPhe1-Tyr3-octreotate (Ga-68 DOTATATE) – one of the positron-emitting radionuclide tracers which has affinity to neuroendocrine tumors by binding to SSTR receptors.

Mean SUV – average SUV counts in the whole lesion.

Peptide Receptor Radionuclide Therapy (PRRT) – A targeted treatment using Lutetium-177 DOTATATE for neuroendocrine tumors which takes advantage of somatostatin receptor overexpression in these tumors.

Positron emission tomography (PET) – an imaging modality which uses positron emission of a radionuclide with preferential binding to select diseases either based on metabolic/molecular activity of the lesions or the presence of certain receptors.

Standardized uptake value (SUV) – a semiquantitative measurement of radiopharmaceutical uptake of a lesion normalized to dose/radioactivity administered and volume of distribution in the body (weight or lean body mass).

SUV maximum (SUVmax) – highest SUV value in a given lesion.

SUV ratio (SUVr or SUVratio) – ratio of the SUV max of a lesion and mean SUV of the liver or spleen.

Total lesion activity (TLA) – molecular tumor volume multiplied by the mean SUV.

Molecular tumor volume (MTV) – areas of the tumor demonstrating increased radiopharmaceutical uptake.

SUV average (SUVav) – sum of the SUV maximum of up to five lesions with the highest radiopharmaceutical uptake divided by number of identified hottest lesions.

Description of Study Procedure

A retrospective correlational study of patients who have biopsy-proven well-differentiated neuroendocrine tumors and who underwent at least two Ga-68 DOTATATE PET-CT scans with interval treatment in St. Luke's Medical Center Quezon City and Global City.

Scan Retrieval and Data Consolidation

Retrieval of scans (DICOM images) and official reports from PACS Carestream database of both branches of the hospital was done. A data collection form was filled out by the principal investigator assigning each patient a code. The readers to re-evaluate the scans were blinded to the patients' identity and clinical status, the medical, surgical and/or nuclear oncologists and treatment modalities.

Analysis of Images

Measurement of tumor volumes on diagnostic CT and SUV values and SUV ratios of each scan were done by two radiologists and two nuclear medicine physicians who have at least 4 years of experience in their respective fields.

All SUVs were normalized to the patient's body weight. The mean liver SUV was acquired by drawing a 3-cm region of interest (ROI) in the inferior liver lobe that is free of disease. The ROI was decreased up to 1-cm if disease in the liver is too severe to acquire 3-cm diameter ROI. The mean spleen SUV is acquired by drawing a 2-cm ROI in the area of the spleen with the highest uptake. The hottest lesion in each scan is defined as the lesion with the highest SUVmax value. This was manually identified in each of the scan. To acquire the molecular tumor volume and total lesion activity, readers drew an ROI over an identified lesion using the RECIST-VOI feature of Siemens syngo.via application (Siemens Healthineers, Germany). Manual adjustment was made to avoid regions with physiologically elevated tracer uptake. SUV thresholds were adjusted for each scan by each of the readers as they deemed fit to accommodate the differences in the activities of tracer administered and length of acquisition.

The SUVmax of the hottest lesion was used to analyze baseline and follow-up values and percentage change for SUVmax, SUVav and tumor-to-mean liver and tumor-to-mean spleen ratios. The tumoral SUVav was calculated as the average of the SUVmax of up to five of the hottest lesions in the scan. Molecular tumor volume and total lesion activity were also derived. The average SUV and SUVr values and RECIST response were averaged from two readers

Using the RECIST 1.1 criteria for tumor response as standard, we assessed significant change in quantitative SUVs and SUV ratios to predict response to chemotherapy, somatostatin analogue therapy and PRRT.

Obtaining Quantitative Parameters

The aforementioned data were manually recorded into a data collection form and also encoded into a spreadsheet for documentation and computation.

Description of Outcome Measures

The primary outcome of this study is the determination of SUV parameter cut-off values whether SUV max or SUVrs which can predict good response to therapy.

The secondary outcomes are the comparability of SUV quantitative parameters versus RECIST 1.1 criteria to assess treatment response.

A binary response criteria is used. Response is defined as having stable disease or regression while non-response will be those with disease progression.

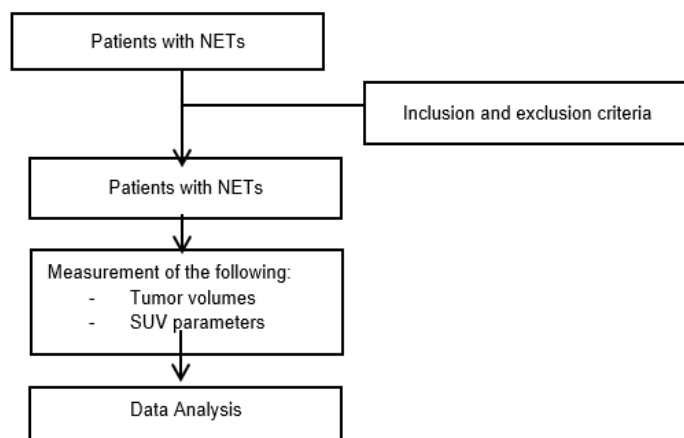


FIGURE 1. Study Methodology

Sample Size Estimation

At 95% confidence level and 80% power of test, minimum sample size needed to evaluate the predictive ability of Ga-DOTATE PET/CT parameters to PRRT response is at least 17 patients. Expected frequency is 11 responding and 6 non-responding. The computation is based on the resulting Area under the curve of 0.87 of SUVmax from the results of the study of Kratochwil [14].

Statistical Methodology

Descriptive statistics such as mean and standard deviation was used to present continuous data. In comparing the baseline and the percentage of change, among different treatment modalities, One Way ANOVA was utilized. Diagnostic accuracy such as sensitivity and specificity and AUC was also utilized to determine the discriminatory

ability of the variables in discriminating progression disease response to other response.

RESULTS

A total of 88 patients with Ga-68 DOTATATE PET/CT scans were retrieved from the existing databases in St. Luke's Medical Center Quezon City and Global City from 2018 until September 9, 2023. For patients who had more than two DOTATATE PET/CT scans, the first two scans whose PET and CT scans were simultaneously acquired were used. Only 19 patients diagnosed with neuroendocrine tumor (13 male, 6 female) satisfied the inclusion and exclusion criteria and were included in the study wherein 31.58% of them were treated with PRRT while 31.58% were treated with octreotide (Table 1). The other 15.79% were given chemotherapy and 10.53% had combination of octreotide and chemotherapy. One patient had combination of partial resection, PRRT, octreotide and chemotherapy in between the DOTATATE PET/CT scans (Table 2).

TABLE 1. Patients Baseline Characteristics

	Values
Age (years), mean	55.5
Gender,	
Male	13 (68%)
Female	6 (32%)
Location of NET	
Gastrointestinal	5 (26%)
Pancreatic	9 (48%)
Others	5 (26%)

TABLE 2. Number of Patients per Treatment Modality

Treatment Modality	%
Chemotherapy	3 (15.79%)
Octreotide	6 (31.58%)
Octreotide + PRRT	2 (10.53%)
PRRT	6 (31.58%)
Surgery + PRRT + Octreotide + Chemotherapy	1 (5.26%)
Surgery only	1 (5.26%)

Comparison of Ga-68 PET-CT SUV Parameters Between Treatments

There is no significant difference in the mean baseline values of the following parameters between treatment modalities: SUVmax, Tumor-to- mean liver SUVr, Tumor-

to- mean spleen SUVR, Tumor SUV av, MTV and TLA (Tables 3A—3F). Although not significant, patients treated by octreotide and PRRT has the highest SUV max baseline of 94.76. Moreover, though not significant, highest baseline mean tumor-to-mean liver and tumor-to-mean spleen SUVRs are among those treated with octreotide combined with PRRT- 15.91 and 6.43, respectively while highest mean tumor SUV av baseline (96.09) is seen among patients given PRRT only. The mean MTV baseline highest mean (207.94) is seen in the patient who underwent surgery, PRRT, Octreotide and chemotherapy. The resulting mean TLA baseline (4383.63) is highest in the octreotide arm.

TABLE 3A. Baseline SUVmax

Treatment Modality	Mean \pm SD
Chemotherapy	21.34 \pm 7.00
Octreotide	52.93 \pm 31.81
Octreotide + PRRT	94.76 \pm 71.63
PRRT	65.09 \pm 38.39
Surgery + PRRT + Octreotide + Chemotherapy	46.91
Surgery only	20.52

p-value = 0.345

TABLE 3B. Baseline Tumor-to- mean liver SUVR

Treatment Modality	Mean \pm SD
Chemotherapy	5.14 \pm 3.61
Octreotide	8.04 \pm 31.81
Octreotide + PRRT	15.91 \pm 15.75
PRRT	10.50 \pm 6.11
Surgery + PRRT + Octreotide + Chemotherapy	46.91
Surgery only	20.52

p-value = 0.498

TABLE 3C. Baseline Tumor-to- mean spleen SUVR

Treatment Modality	Mean \pm SD
Chemotherapy	2.59 \pm 0.86
Octreotide	4.17 \pm 3.05
Octreotide + PRRT	6.43 \pm 2.71
PRRT	4.17 \pm 3.61
Surgery + PRRT + Octreotide + Chemotherapy	2.61
Surgery only	1.36

p-value = 0.713

TABLE 3D. Baseline Tumor SUV av

Treatment Modality	Mean \pm SD
Chemotherapy	21.67 \pm 10.23
Octreotide	27.85 \pm 12.78
Octreotide + PRRT	61.41 \pm 32.27
PRRT	96.09 \pm 119.84
Surgery + PRRT + Octreotide + Chemotherapy	46.91
Surgery only	5.28

p-value = 0.624

TABLE 3E. Baseline MTV

Treatment Modality	Mean \pm SD
Chemotherapy	11.70 \pm 8.27
Octreotide	142.61 \pm 275.68
Octreotide + PRRT	128.50 \pm 127.33
PRRT	66.94 \pm 136.22
Surgery + PRRT + Octreotide + Chemotherapy	207.94
Surgery only	74.37

p-value = 0.910

TABLE 3F. Baseline TLG

Treatment Modality	Mean \pm SD
Chemotherapy	107.35 \pm 84.26
Octreotide	4383.63 \pm 9602.91
Octreotide + PRRT	3891.08 \pm 5374.43
PRRT	948.17 \pm 1946.09
Surgery + PRRT + Octreotide + Chemotherapy	3645.89
Surgery only	713.67

p-value = 0.898

Interval Changes in the Ga-68 DOTATATE PET-CT SUV parameters

Tumor SUVmax

Results show that mean percentage of change in SUVmax baseline displayed an increase of 71.9% among patients treated with chemotherapy. This implies that the mean follow-up is higher than baseline. On the other hand, among those treated with PRRT only, the mean percentage of change decreased by 21.74% (Table 4A).

TABLE 4A. Interval Change : SUVmax

Treatment Modality	Mean Change (Follow-up — Baseline) \pm SD
Chemotherapy	71.93 \pm 73.73
Octreotide	23.74 \pm 80.97
Octreotide + PRRT	9.42 \pm 51.48
PRRT	-21.74 \pm 38.47
Surgery + PRRT + Octreotide + Chemotherapy	25.79
Surgery only	-16.70

p-value = 0.487

Tumor-to-mean liver SUVR

The mean percentage of change of the tumor-to-mean liver SUVR is also a positive for chemotherapy (103.31 \pm 1442.46). On the other hand, PRRT-treated patients recorded a negative 14.88 \pm 49.73 change (Table 4B).

TABLE 4B. Interval Change: Tumor-to- mean liver SUVR

Treatment Modality	Mean Change (Follow-up — Baseline) \pm SD
Chemotherapy	103.31 \pm 142.46
Octreotide	89.05 \pm 143.85
Octreotide + PRRT	37.61 \pm 52.53
PRRT	-14.88 \pm 49.73
Surgery + PRRT + Octreotide + Chemotherapy	74.51
Surgery only	62.99

p-value = 0.621

Tumor-to-mean spleen SUVR

The mean percentage of change has increased and is the highest among patients given chemotherapy only at 115.07 \pm 135.11. PRRT-treated patients remain to have a negative percentage of change but only by 6.16 \pm 76.95 (Table 4C).

Tumor SUVav

The highest interval increase in the mean tumor SUV av is 182.98 seen in the patient with partial resection. It is significantly higher than the rest of the other treatments (Table 4D).

TABLE 4C. Interval Change: Tumor-to- mean spleen SUVR

Treatment Modality	Mean Change (Follow-up — Baseline) \pm SD
Chemotherapy	115.07 \pm 135.11
Octreotide	96.11 \pm 166.05
Octreotide + PRRT	30.62 \pm 5.48
PRRT	-6.16 \pm 76.95
Surgery + PRRT + Octreotide + Chemotherapy	39.91
Surgery only	89.09

p-value = 0.711

TABLE 4D. Interval Change: SUVav

Treatment Modality	Mean Change (Follow-up — Baseline) \pm SD
Chemotherapy	71.39 \pm 91.59
Octreotide	24.29 \pm 21.83
Octreotide + PRRT	-15.63 \pm 30.97
PRRT	-5.45 \pm 27.60
Surgery + PRRT + Octreotide + Chemotherapy	25.79
Surgery only	182.98

p-value = 0.015

Molecular Tumor Volume

The resulting mean percentage of change on MTV is highest among patients treated with chemotherapy only (139.80 \pm 226.20). PRRT also resulted to an increase with only 2.74 \pm 22.31. An interval decrease is recorded among patients given octreotide only by 13.49 \pm 36.02 (Table 4E).

TABLE 4E. Interval Change: MTV

Treatment Modality	Mean Change (Follow-up — Baseline) \pm SD
Chemotherapy	139.80 \pm 226.20
Octreotide	-13.49 \pm 36.02
Octreotide + PRRT	-36.68 \pm 4.96
PRRT	2.74 \pm 22.31
Surgery + PRRT + Octreotide + Chemotherapy	-31.85
Surgery only	-56.39

p-value = 0.253

Total Lesion Activity

TLA mean change in percentage is positive and is highest among chemotherapy treated patients (261.26 ± 390.12) (Table 4F).

TABLE 4F. Interval Change: TLA

Treatment Modality	Mean Change (Follow-up — Baseline) ± SD
Chemotherapy	261.26 ± 390.12
Octreotide	3.76 ± 57.77
Octreotide + PRRT	-72.16 ± 25.62
PRRT	-19.01 ± 48.35
Surgery + PRRT + Octreotide + Chemotherapy	-28.78
Surgery only	-56.38

p-value = 0.711

Among the different variables, only MTV and TLA baseline turns out to be significant. Specifically, they can significantly discriminate a progressive disease and non-progressive disease as their area under the curve of 0.782 (95% CI : 0.56 to 1.0) and 0.808 (95% CI : 0.58 to 1.0) are significant with resulting p - value of 0.013 and 0.008, respectively. Though both significant, TLA turns out to be the better predictor as it resulted to both acceptable sensitivity of 66.7% (95% CI : 22.3% to 95.7%) and specificity of 92.3% (95% CI : 64% to 99.8%). On the other hand, MTV baseline has only 53.8% specificity (95% CI : 25.1 to 80.8) (Table 5).

DISCUSSION

Our study shows the potential of using molecular tumor volume (100% sensitivity, 53.8% specificity, AUC 0.82) and total lesion activity (66.7% sensitivity, 92.3% specificity, AUC 0.808) with values less than 37.76 cm^3 and $60.95\text{ SUV} \cdot \text{cm}^3$ to predict poor response to

treatment. This highlights the importance of having adequate somatostatin receptor density for treatment response in NETs. However, the response for each of the treatment modality cannot be assessed due to the small number of our population.

Although not significant, in those patients treated with PRRT alone and in combination with other treatment, there was either consistent decline in the values of SUVmax, SUVav, and tumor-to-mean liver and tumor-to-mean spleen SUVr or these patients present with the lowest interval increase.

The aforementioned DOTATATE PET parameters may serve as a guide to clinicians whether to initiate, continue or augment a certain treatment and perhaps to do closer monitoring.

With the increasing number of PET centers in the country, the use of PET/CT scans to stage and monitor disease will be more inexpensive and attainable. With the advent of PRRT in the country which gave another option for management of neuroendocrine tumors, the use and availability of Ga-68 DOTATATE PET/CT scans will be greater.

Limitations of the study and Future Recommendations

Ga-68 DOTATATE PET/CT scans are relatively new in the country, made available only in 2018. There is limited available of this procedure, being offered only in St. Luke’s Medical Center and is significantly more expensive than conventional imaging modalities. Selection bias also possibly plays a role in this study since only those able to afford the scan and subsequent treatment were included. These resulted in a small sample size.

TABLE 5. Cut-off values for each SUV parameter

Baseline Parameters	Best Cut-off	Sensitivity (95% CI)	Specificity (95% CI)	AUC (95% CI)	p-value
SUVMax	≤ 32.55	66.7 (22.3 - 95.7)	69.2 (38.6 - 90.9)	0.625 (0.32 - 0.92)	0.452
Tumor-to- mean liver SUVr	≤ 4.24	50.0 (11.8 - 88.2)	84.6 (54.6 - 98.1)	0.577 (0.26 - 0.89)	0.630
Tumor-to-mean spleen SUVr	≤ 3.57	83.3 (35.9 - 99.6)	46.2 (19.2 - 74.9)	0.603 (0.33 - 0.88)	0.462
Tumor SUV av	≤ 33.24	83.3 (35.9 - 99.6)	61.5 (31.6 - 86.1)	0.590 (0.28 - 0.90)	0.569
MTV	≤ 37.76	100.0 (54.1 - 100)	53.8 (25.1 - 80.8)	0.782 (0.56 - 1.00)	0.013
TLA	≤ 60.95	66.7 (22.3 - 95.7)	92.3 (64 - 99.8)	0.808 (0.58 - 1.00)	0.008

Automated PET tumor segmentation software is also not available in both centers hence readers resorted to identifying lesions with the highest SUV uptake manually including measurements of tumor volume. This did not allow slice-by-slice identification and tumoral/lesion borders.

To increase the power of the study, the authors propose a much bigger sample size. A more in-depth analysis would involve stratifying patients into stable disease, progressive disease, partial and complete response. Sub-analysis of treatment modalities per origin and grading of tumors would also be possible and will be helpful in the decision-making of clinicians. A prospective study would also generate more information and will be able to assess the potential of DOTATATE PET parameters to predict progression-free and overall survival of Filipino patients diagnosed with NETs.

Should more advanced software be made available, a more objective and uniform way of acquiring SUV parameters would also be possible.

Ethical Considerations

The Clinical Protocol and all relevant documents were reviewed and approved by the SLMC Institutional Ethics Review Committee. The study abided by the Principles of the Declaration of Helsinki (2013) and was conducted along the Guidelines of the International Conference on Harmonization-Good Clinical Practice (ICH-GCP).

The anonymity of patients and their records were ensured by coding each of the scans and data collection forms and their treatment modalities were not disclosed. All study-related documents such as all the versions of the protocol, ethical clearance, data collection forms, and hard copies of source documents are kept and stored by the Principal Investigator in strict confidentiality and will be so for at least 5 years, after which they will be shredded. Should data be in electronic form, it will be stored in the investigators' personal laptop with password protection and a Google drive with the link given only to investigators involved. It shall be deleted 5 years after the study is completed. All documents and related information to the study were made available for audit at any time the IERC deems fit.

REFERENCES

1. Scalettar, B. A., Jacobs, C., Fulwiler, A., Prahl, L., Simon, A., Hilken, L., & Lochner, J. E. (2012). Hindered submicron mobility and long-term storage of presynaptic dense-core

granules revealed by single-particle tracking. *Developmental neurobiology*, 72(9), 1181–1195. <https://doi.org/10.1002/dneu.20984>.

2. Inzani, F., & Rindi, G. (2021). Introduction to neuroendocrine neoplasms of the digestive system: definition and classification. *Pathologica*, 113(1), 1–4. <https://doi.org/10.32074/1591-951X-227>.
3. Rindi, G., Mete, O., Uccella, S., Basturk, O., La Rosa, S., Brosens, L. A. A., Ezzat, S., de Herder, W. W., Klimstra, D. S., Papotti, M., & Asa, S. L. (2022). Overview of the 2022 WHO Classification of Neuroendocrine Neoplasms. *Endocrine pathology*, 33(1), 115–154. <https://doi.org/10.1007/s12022-022-09708-2>.
4. Hallet, J., Law, C. H., Cukier, M., Saskin, R., Liu, N., & Singh, S. (2015). Exploring the rising incidence of neuroendocrine tumors: a population-based analysis of epidemiology, metastatic presentation, and outcomes. *Cancer*, 121(4), 589–597. <https://doi.org/10.1002/cncr.29099>.
5. Taal, B. G., & Visser, O. (2004). Epidemiology of neuroendocrine tumours. *Neuroendocrinology*, 80 Suppl 1, 3–7. <https://doi.org/10.1159/000080731>.
6. Raphael, M. J., Chan, D. L., Law, C., & Singh, S. (2017). Principles of diagnosis and management of neuroendocrine tumours. *CMAJ : Canadian Medical Association journal = journal de l'Association medicale canadienne*, 189(10), E398–E404. <https://doi.org/10.1503/cmaj.160771>.
7. Sanli, Y., Garg, I., Kandathil, A., Kendi, T., Zanetti, M. J. B., Kuyumcu, S., & Subramaniam, R. M. (2018). Neuroendocrine tumor diagnosis and management: 68Ga-DOTATATE PET/CT. *AJR. American Journal of Roentgenology*, 211(2), 267–277. <https://doi.org/10.2214/ajr.18.19881>.
8. Gabriel, M., Decristoforo, C., Kendler, D., Dobrozemsky, G., Heute, D., Uprimny, C., Kovacs, P., Von Guggenberg, E., Bale, R., & Virgolini, I. J. (2007). 68Ga-DOTA-Tyr3-octreotide PET in neuroendocrine tumors: Comparison with somatostatin receptor scintigraphy and CT. *Journal of Nuclear Medicine: Official Publication, Society of Nuclear Medicine*, 48(4), 508–518. <https://doi.org/10.2967/jnumed.106.035667>.
9. Deppen, S. A., Liu, E., Blume, J. D., Clanton, J., Shi, C., Jones-Jackson, L. B., Lakhani, V., Baum, R. P., Berlin, J., Smith, G. T., Graham, M., Sandler, M. P., Delbeke, D., & Walker, R. C. (2016). Safety and efficacy of 68Ga-DOTATATE PET/CT for diagnosis, staging, and treatment management of neuroendocrine tumors. *Journal of Nuclear Medicine*, 57(5), 708–714. <https://doi.org/10.2967/jnumed.115.163865>.
10. Kulke MH, Siu LL, Tepper JE, Fisher G, Jaffe D, Haller DG, Ellis LM, Benedetti JK, Bergsland EK, Hobday TJ, Van Cutsem E, Pingpank J, Oberg K, Cohen SJ, Posner MC, Yao JC. Future directions in the treatment of neuroendocrine tumors: consensus report of the National Cancer Institute Neuroendocrine Tumor clinical trials planning meeting. *J Clin Oncol*. 2011 Mar.

11. Oronsky, B., Ma, P. C., Morgensztern, D., & Carter, C. A. (2017). Nothing But NET: A Review of Neuroendocrine Tumors and Carcinomas. *Neoplasia* (New York, N.Y.), 19 (12), 991–1002. <https://doi.org/10.1016/j.neo.2017.09.002>.
12. Bautista P. A. (2019). The Emergence of Theranostics in the Philippines: Overcoming Challenges and Bringing Hope. *Nuclear medicine and molecular imaging*, 53(1), 30–32. <https://doi.org/10.1007/s13139-018-0560-7>.
13. Ruchalski, K., Dewan, R., Sai, V., McIntosh, L. J., & Braschi-Amirfarzan, M. (2022). Imaging response assessment for oncology: An algorithmic approach. *European journal of radiology open*, 9, 100426. <https://doi.org/10.1016/j.ejro.2022.100426>.
14. Kratochwil, C., Stefanova, M., Mavriopoulou, E., Holland-Letz, T., Dimitrakopoulou-Strauss, A., Afshar-Oromieh, A., Mier, W., Haberkorn, U., & Giesel, F. L. (2015). SUV of [68Ga]DOTATOC-PET/CT predicts response probability of PRRT in neuroendocrine tumors. *Molecular Imaging and Biology: MIB: The Official Publication of the Academy of Molecular Imaging*, 17(3), 313–318. <https://doi.org/10.1007/s11307-014-0795-3>.
15. Lee, H., Eads, J. R., & Pryma, D. A. (2021). 68 Ga-DOTATATE Positron Emission Tomography-Computed Tomography Quantification Predicts Response to Somatostatin Analog Therapy in Gastroenteropancreatic Neuroendocrine Tumors. *The oncologist*, 26(1), 21–29. <https://doi.org/10.1634/theoncologist.2020-0165>.
16. Sharma, R., Wang, W. M., Yusuf, S., Evans, J., Ramaswami, R., Wernig, F., Frilling, A., Mauri, F., Al-Nahhas, A., Aboagye, E. O., & Barwick, T. D. (2019). 68Ga-DOTATATE PET/CT parameters predict response to peptide receptor radionuclide therapy in neuroendocrine tumours. *Radiotherapy and oncology : journal of the European Society for Therapeutic Radiology and Oncology*, 141, 108–115. <https://doi.org/10.1016/j.radonc.2019.09.003>.
17. Sharma, P., Naswa, N., Kc, S. S., Alvarado, L. A., Dwivedi, A. K., Yadav, Y., Kumar, R., Ammini, A. C., & Bal, C. (2014). Comparison of the prognostic values of 68Ga-DOTANOC PET/CT and 18F-FDG PET/CT in patients with well-differentiated neuroendocrine tumor. *European journal of nuclear medicine and molecular imaging*, 41 (12), 2194–2202. <https://doi.org/10.1007/s00259-014-2850-3>.
18. Pauwels, E., Dekervel, J., Verslype, C., Clement, P. M., Dooms, C., Baete, K., Goffin, K., Jentjens, S., Van Laere, K., Van Cutsem, E., & Deroose, C. M. (2022). [68Ga]Ga-DOTATATE-avid tumor volume, uptake and inflammation-based index correlate with survival in neuroendocrine tumor patients treated with [177Lu]Lu-DOTATATE PRRT. *American journal of nuclear medicine and molecular imaging*, 12(5), 152–162.

Occult Breast Cancer: A Case Report

Belinda R. Dancel-San Juan, MD, MSc

Careview PET/CT Center - Mary Mediatrix Medical Center

E-mail address: belinda.sanjuan@gmail.com

ABSTRACT

Patients with occult breast cancer present with axillary lymphadenopathy and no evidence of a primary breast lesion. This rare type of cancer is a diagnostic and therapeutic challenge. This is a case of a 50 year old female presenting with a two year history of palpable axillary lymphadenopathy. Mammography and ultrasound showed masses in the left breast and left axilla. Subsequent biopsy of these lesions showed invasive carcinoma in the left axillary mass while the left breast lesion was benign. Further evaluation using PET-CT and molecular breast imaging showed no evidence of lesion in the ipsilateral breast and remainder of the body. PET-CT is also used to determine any possible sites of primary lesion in the body. The roles of PET-CT and molecular breast imaging are discussed with regards to its importance in the evaluation and use in the management of a patient with occult breast cancer.

Keywords: occult breast cancer, FDG PET-CT, molecular breast imaging

INTRODUCTION

Breast cancer is one of the most common types of cancer and a leading cause of cancer death among women. In 2022, there were 2.3 million women diagnosed with breast cancer globally and 33,079 diagnosed in the Philippines [1,2]. There were 670,000 deaths globally and 11,857 deaths in the Philippines [1,2].

Occult breast cancer is a rare type of cancer presenting with axillary lymphadenopathy with no clinical or radiological evidence of a primary breast lesion. Even though breast cancer is the most common cancer in females, only less than 1% of cases present with occult breast cancer [3].

Imaging plays an important role in the evaluation of breast cancer and will help in determining the appropriate management for the patient. Mammography is the recommended imaging modality in the evaluation of breast cancer and ultrasound is recommended if necessary [4]. Positron emission tomography-computed tomography (PET-CT), CT scan of the chest, abdomen and pelvis plus bone scan determine

systemic staging. PET-CT staging with F18 fluorodeoxyglucose (FDG) may replace CT scan of the chest, abdomen and pelvis plus bone scan to assess metastatic disease [5].

Molecular breast imaging using Technetium 99m (Tc99m) sestamibi is a complementary imaging tool that is useful in patients with dense breasts, presence of breast implants or prior breast surgery and radiation [6].

This case report will present the imaging findings and management of a patient diagnosed to have occult breast cancer.

CASE PRESENTATION

This case presents a 50 year old female with a two year history of a palpable left axillary mass. It was firm, movable and not painful on clinical examination. The patient did not present with any signs or symptoms of infection or inflammation during this time. She has a family history of breast cancer (mother and maternal aunt). Mammogram showed a mass in the left axilla measuring 3.5 x 3.0 cm (Figure 1). Ultrasound done on the same day showed a lobulated, hypoechoic left

axillary mass measuring 3.19 x 2.5 x 2.54 cm corresponding to the left axillary mass seen in mammogram. Additionally there was a hypoechoic mass in the left breast measuring 0.94 x 0.82 x 1.04 cm. Tissue correlation was suggested for these lesions .

Subsequent ultrasound-guided core needle biopsy of both the left axillary and left breast masses were done. The left axillary mass showed invasive carcinoma of no special type with medullary pattern. There was no lymphovascular space invasion identified. The left breast mass showed fibrocystic changes. Immunohistochemical staining determined the left axillary mass to be hormone positive (ER/PR) and Her2 negative.

Molecular breast imaging was requested for further evaluation. This showed a sestamibi-avid lesion in the left axillary region. There were no sestamibi-avid lesions seen in either breast and right axillary region (Figure 2).

PET-CT scan was also requested for further workup and to determine presence of distant metastasis. The study showed an FDG-avid left axillary mass (Figure 3). There were no discrete mass or FDG-avid focus seen in the bilateral breasts and axillary areas. There was no evidence of distant metastasis.

The patient underwent left modified radical mastectomy. The left axillary tumor measured 3.5 cm in greatest dimension and the histopathologic diagnosis was invasive carcinoma with medullary features. Extensive examination of the breast revealed no tumors in the breast proper. There were additional 24 lymph nodes identified and all were negative for metastasis. The patient was subsequently given chemotherapy and radiation therapy. Follow-up mammograms showed no suspicious mammographic findings.

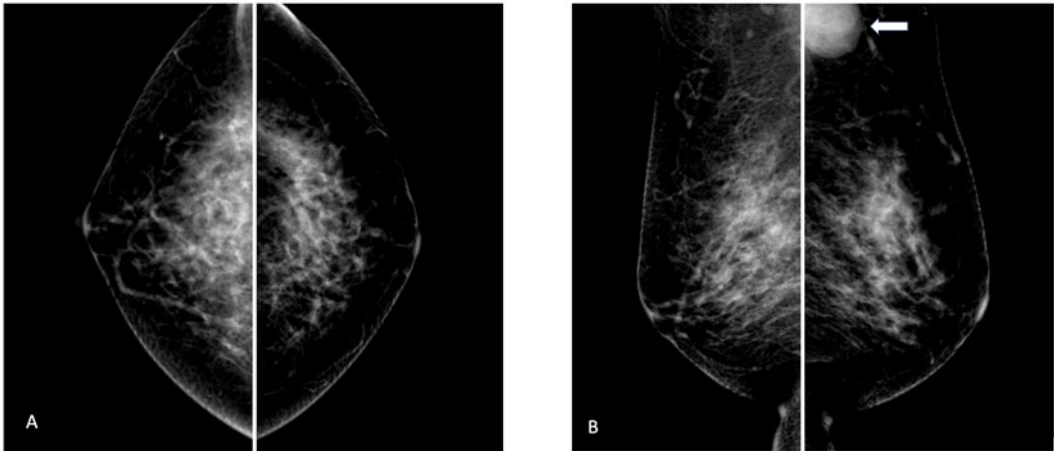


FIGURE 1. Mammogram obtained from the craniocaudal (Panel A) and mediolateral oblique (Panel B) views show a mass in the left axillary region.

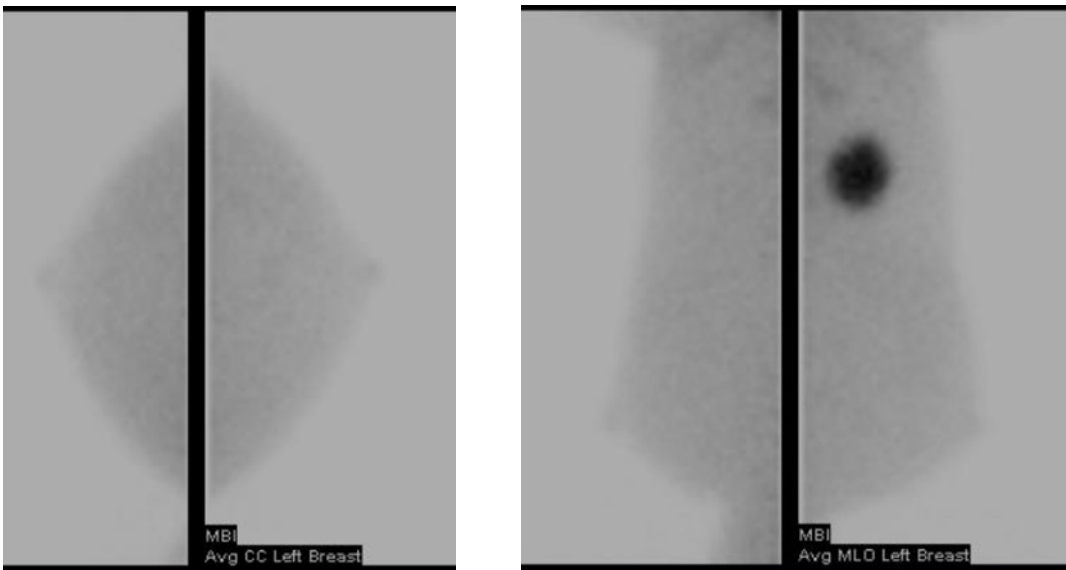


FIGURE 2. Molecular breast imaging obtained from the craniocaudal (A) and mediolateral oblique (B) views show a sestamibi-avid lesion in the left axillary region.

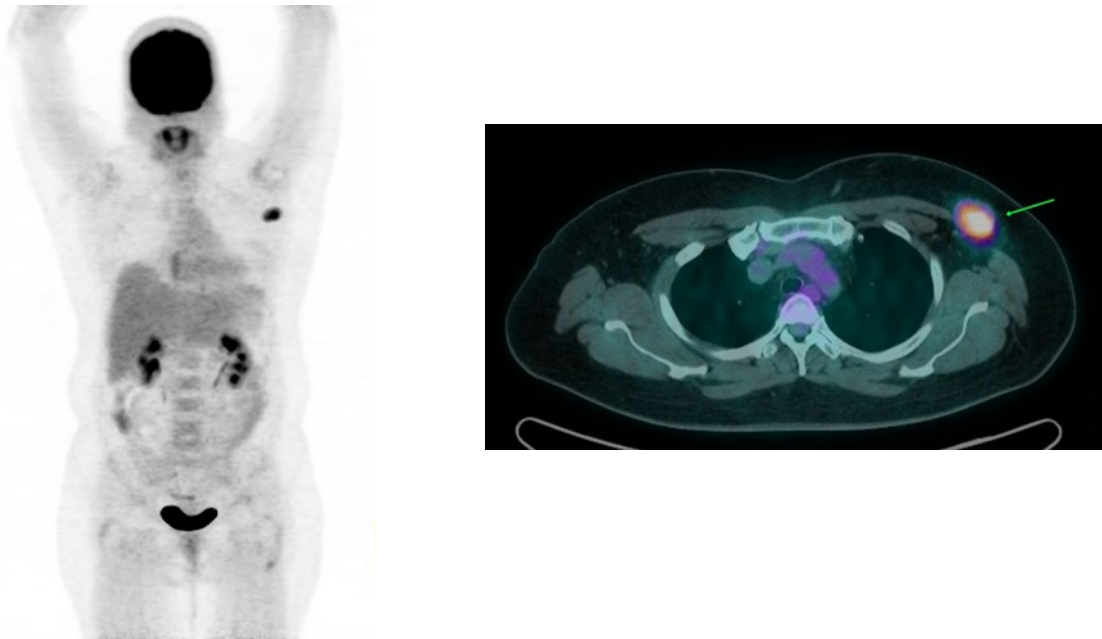


FIGURE 3. Maximum intensity projection of PET-CT (A) and fused PET-CT image (B) show an FDG-avid left axillary mass.

DISCUSSION

It is important to determine the etiology of patients who present with axillary lymphadenopathy. In general, lymph nodes seen in any anatomic site is most likely due to a benign etiology [7]. However, this patient did not present with any clinical signs or symptoms of an infection or inflammation.

Malignancy was entertained as the cause of the patient's two year history of a palpable axillary mass. While the most common malignant cause of persistent axillary lymphadenopathy is lymphoma, the breast is the most common primary tumor location in women [8]. Therefore, an important diagnosis to consider in female patients presenting with axillary lymphadenopathy is breast cancer. Along with physical examination, the patient underwent several imaging modalities in the evaluation of the left axillary mass and to determine the possible origin of the primary lesion.

Physical examination and imaging using mammography and breast ultrasound are used in the initial evaluation of breast cancer [4]. Breast MRI is optional and may help in the identification and management of clinically occult primary tumors presenting with axillary nodal metastases [4]. Molecular breast imaging is used as a complementary imaging tool in patients with newly diagnosed breast cancer. It can help evaluate extent, multicentricity when breast MRI is not available or cannot be performed [6]. Since imaging with Tc99m

sestamibi is independent of breast density, this can be used in patients with dense breasts, presence of breast implants or prior breast surgery and radiation [6]. Molecular imaging done in this patient showed a sestamibi-avid lesion in the left axillary region. It has been shown that the uptake and retention of Tc99m sestamibi is related to the level of tissue metabolism and tumor size and type [6].

Conventional imaging for the evaluation of distant metastasis includes anatomic imaging using CT and functional imaging to evaluate bone involvement using bone scintigraphy [9]. On the other hand, PET-CT imaging provides both anatomic and functional imaging and is used to determine lymph node involvement and the presence of distant metastasis. PET-CT is most helpful in cases where standard imaging studies are equivocal or suspicious, especially in the setting of locally advanced or metastatic disease [4]. PET studies are used to evaluate FDG-avid foci in mammographically occult breast cancer patients [10]. In this case, PET-CT imaging is done to confirm the absence of a breast lesion and to determine presence of distant metastasis. This is also used to evaluate for other potential sites of a primary lesion that would present as abnormal axillary lymphadenopathy.

Occult breast cancer is a rare type of cancer with a very low incidence rate. The most common clinical presentation of occult breast cancer is an axillary mass [10]. Biopsy done on the left axillary mass confirmed the diagnosis of malignancy. In the absence of a lesion in the

ipsilateral breast, this supported the diagnosis of occult breast cancer. The patient underwent left modified radical mastectomy. Extensive examination of the breast revealed no tumors in the breast proper and the axillary tumor appears to be carcinoma with medullary features within a lymph node. Studies suggest that occult breast cancer may originate from ectopic breast tissue that is present in axillary lymph nodes, which may undergo proliferative changes and may also undergo malignant transformation [11]. Immunohistochemical staining done on the left axillary tumor showed hormone positive (ER/PR) and Her2 negative.

It has been shown that the characteristics of patients with occult breast cancer are comparable to patients with stage II to III breast cancer. The prognosis of patients with occult breast cancer is determined to be equivalent or slightly better than patients with stage II to III breast cancer [10, 12, 13]. Generally, treatment of occult breast cancer is similar to that of primary breast cancer with axillary lymph node involvement. Several studies showed that even though there are no detectable lesions in the breast, modified radical mastectomy or breast conserving surgery with radiotherapy can further improve the survival and prognosis of patients with occult breast cancer [12 - 14]. It was determined that having local treatment of the breast showed a better overall survival and recurrence-free survival compared to observation [15]. Subsequent chemotherapy, endocrine therapy and targeted therapy will depend on the molecular type and clinical stage of the patient [14].

CONCLUSION

When presented with a case of metastatic axillary lymphadenopathy, the next step is to determine where the primary lesion. Aside from conventional imaging, nuclear medicine procedures play an important role in the management of breast cancer. Both PET-CT scan and molecular breast imaging helped determine the absence of a primary lesion within the breast. PET-CT scan has an added advantage of being able to image the whole body and was able to confirm the absence of distant metastasis. It is also used to determine any possible sites of primary lesion in the body. Information obtained from both of these imaging modalities helped to determine the appropriate management plan for the patient.

Informed Consent

Informed consent was obtained from the patient for the

purpose of publishing this case report .

REFERENCES

1. World Health Organization: Breast Cancer. Available from: <https://www.who.int/news-room/fact-sheets/detail/breast-cancer>.
2. World Health Organization Global Cancer Observatory: Philippines. Available from: <https://gco.iarc.who.int/media/globocan/factsheets/populations/608-philippines-fact-sheet.pdf>.
3. Espino AA, Bernal IC, Guarecuco JE, El-Tawil R, Masri MM. Adenocarcinoma of the breast presenting as occult breast cancer with axillary and supraclavicular lymph node metastasis: a case report. *Cureus* 2023;15(5):e39583.
4. Gradishar WJ, Moran MS, Abraham J, Aft R, Agnese D, Allison KH, et al. Breast cancer, version 3.2022, NCCN clinical practice guidelines in oncology. *Journal of the National Comprehensive Cancer Network* 2022;20(6): 691-722.
5. Groheux D, Cochet A, Humbert O, Alberini JL, Hindié E, Mankoff D. ¹⁸F-FDG PET/CT for staging and restaging of breast cancer. *J Nucl Med* 2016 Feb;57 Suppl 1:17S-26S.
6. Muzahir S. Molecular breast cancer imaging in the era of precision medicine. *AJR* 2020;215:1512-1519.
7. Harris Pierce E, Gray HK, Dockerty MB. Surgical significance of isolated axillary adenopathy. *Ann Surg* 1957;145:104-107.
8. Brenin DR. The unknown primary tumor presenting with axillary lymphadenopathy. In: Singletary SE, Robb GL, Hortobagyi GN, eds. *Advanced Therapy of breast disease*. London: BC Decker Inc 2004;659-665.
9. Ulaner GA. PET/CT for patients with breast cancer: where is the clinical impact? *AJR* 2019;213:254-265.
10. Wang X. Presentation of axillary metastases from occult breast carcinoma. *Chinese Journal of Clinical Oncology* 2007 Feb;4(1):1-5.
11. Terada M, Adachi Y, Sawaki M, Hattori M, Yoshimura A, Naomi G, et al. Occult breast cancer may originate from ectopic breast tissue present in axillary lymph nodes. *Breast Cancer Res Treat* 2018;172(6):1-7.
12. Ge LP, Liu XY, Xiao Y, Gou ZC, Zhao S. Clinicopathological characteristics and treatment outcomes of occult breast cancer: A SEER population-based study. *Cancer Manag Res* 2018;10(9):4381-91. doi: 10.2147/CMAR.S169019.
13. Vlastos G, Jean M, Mirza AN, et al. Feasibility of breast preservation in the treatment of occult primary carcinoma presenting with axillary metastases. *Ann Surg Oncol* 2001;8:425-431.
14. Wang R, Yang HX, Chen J, Huang JJ, Lv Q. Best treatment options for occult breast cancer: a meta-analysis. *Front Oncol* 2023;13:1051232.
15. Foroudi F, Tiver KW. Occult breast carcinoma presenting as axillary metastases. *Int J Radiat Oncol Biol Phys* 2000;47:143-147.

F18-FDG PET-CT of Takayasu's Arteritis with Large Vessel Morphologic Changes in a Filipino Patient

Carlo Jose S. San Juan, MD

Section of Nuclear Medicine, Department of Radiology, Cardinal Santos Medical Center

E-mail address: calduckmd@yahoo.com

ABSTRACT

This is a case of a 24 year-old Filipino female, with a 10-year history of various non-specific symptoms such as dyspnea, easy fatigability, and fever until she was eventually recently diagnosed with Takayasu's Arteritis. F18-FDG PET-CT was done which showed heterogeneously high-level uptake in the arch of the aorta with morphologic changes such as dilatation of the ascending aorta and arch of the aorta. Segmental calcified mural plaques were observed along the rest of the thoracic and abdominal aorta. Prominence of the right common carotid artery and main pulmonary artery were likewise noted. These were suggestive of an advanced phase of Takayasu's Arteritis.

F18-FDG PET-CT has been shown to have great value in diagnosing Takayasu's Arteritis in its early and active phases, however less has been documented regarding the utility of SUV monitoring in advanced cases which may be a worthwhile premise for future studies.

INTRODUCTION

Takayasu arteritis (TKA), an inflammatory and stenotic disease of medium- and large-sized arteries with a strong predilection for the aortic arch and its branches, is an uncommon disease most prevalent in adolescent girls and young women and mostly occurring in Asia, though no definite racial or geographic restriction has been determined [1].

A granulomatous vasculitis, TKA is characterized principally by ocular disturbances and marked weakening of the upper extremity pulses, hence the name "pulseless disease," and manifests with transmural fibrous thickening yielding severe luminal narrowing of the involved arteries [2].

In a descriptive study of case reports [3], TKA was indeed most commonly found in females with an onset age of 13-38 years, an average of 25.5 years. Predominant presentation involved a wide range of symptoms, fever being the most common, followed by claudication and headache. Shortness of breath, weight loss, syncope, and night sweats were less commonly reported. The heavily associated sign of absent or decreased pulse in the upper

extremity was found in 35% of cases in the study.

The non-specific nature of the typical symptoms makes early diagnosis difficult. Thus imaging, particularly characteristic patterns on arteriography, confirms the diagnosis of TKA [1]. Magnetic Resonance (MRI) or computed tomography (CT) arteriography of the aorta and its major branches should be obtained to fully delineate the distribution and degree of arterial disease. Imaging findings that are typical for TKA include irregular vessel walls, stenosis, poststenotic dilatation, aneurysm formation, occlusion, and evidence of increased collateral circulation.

With the growing use of Positron Emission Tomography – Computed Tomography (PET-CT) with Fluorine-18 Fluorodeoxyglucose (F18-FDG) in oncologic, infectious, and inflammatory cases, its application in imaging large vessel vasculitis (LVV), including TKA, has been found to be among the most sensitive and specific [4].

CASE REPORT

Patient, female, 24 years old, was complaining of difficulty of breathing and easy fatigability 10 years prior to consult (PTC). Upon consultation with a pediatrician,

she was reported to have been diagnosed with myocarditis. 8 years PTC, her diagnosis was changed to dilated cardiomyopathy due to unrecalled reasons. 2 months PTC, upon requesting for a medical clearance for undisclosed purposes, she reported being told that she needed an aortic valve replacement. 1 month PTC, she experienced chills with fever with dyspnea and chest heaviness and was admitted to a hospital. On admission, she reported having a systolic blood pressure of over 200 mmHg. The patient was told that she had an infectious process and a non-contrast CT of the chest was performed. The CT-scan report showed centrilobular nodules in the posterior segment of the right upper lobe and minimal reticulonodular opacities in the superior and lateral basal segments of the right lower lobe, attributed to an infectious process with endobronchial component.

However, the CT-scan also noted atherosclerotic disease of the aorta with fusiform aneurysm involving the ascending aorta and dilated brachiocephalic and right common carotid arteries. Utilizing the 2022 American College of Rheumatology / EULAR classification criteria for Takayasu's Arteritis [5], this patient fulfilled the absolute requirements of being less than 60-years old at the time of diagnosis and have evidence of vasculitis (ascending aorta and brachiocephalic artery) on imaging. Additional criteria and their corresponding points were her being of the female sex (+1), presence of angina (+2), involvement of two arterial territories (thoracic aorta and right carotid, +2), giving a score of 5, which were enough points required for the classification of TKA.

The CT-scan also noted enlarged left pulmonary arteries, suggestive of pulmonary arterial hypertension. Cardiomegaly and an atrophic right kidney were also noted.

It is unclear whether the initial presentation of fever was attributed to the pulmonary infection or TKA, or even both. The elevated systolic blood pressure, while not diagnostic of TKA by itself, does support the diagnosis.

The patient was referred to a rheumatologist and cardiologist, who informed the patient of her new diagnosis of TKA. She was discharged upon stabilization of her fever and F18-FDG PET-CT with contrast was then requested to be done as an outpatient for further whole-body evaluation.

The patient was stable and asymptomatic on the day of her PET-CT imaging. On F18-FDG PET-CT imaging (Siemens Biograph), heterogeneous mild FDG uptake are seen along the walls of the arch of the aorta (SUVmax up to 3.0, liver reference SUVmean 2.3) with subtle wall enhancement (Figure 1). There was diffuse dilatation of the ascending (5.5 cm) and arch of the aorta (4.2 cm), with gradual tapering of the latter's distal segment, and a normal-caliber descending aorta (3.0 cm). Segmental calcified mural plaques were also observed along the rest of the thoracic and abdominal aorta. There was also prominence of the right common carotid artery (1.4 cm) and the main pulmonary artery (3.2 cm) with gradual pruning of the latter.

Along with a noted cardiomegaly, the dilated and calcified vessels, and mild FDG uptake and enhancement along the aortic arch may have related to the TKA diagnosis.

Adding the PET-CT finding of abdominal aortic involvement, the patient's 2022 American College of Rheumatology / EULAR classification criteria for Takayasu's Arteritis [5] score would have an additional 4 points (arterial territories involved changes from two to three and abdominal artery involvement), giving a score of 9, which were more than the 5 points required for the classification of TKA.

DISCUSSION

Considering the inflammatory nature of TKA, F18-FDG is expected to have increased uptake in the walls of the likely affected large and medium-sized vessels even before any morphological abnormalities develop [6], and thus, PET-CT may be a promising tool for early diagnosis [7] and even incidental discovery through the modality's more common applications, such as in oncology [8]. Furthermore, F18-FDG PET-CT has been found to be useful in diagnosing TKA in cases of fever-of-unknown-origin and other non-specific symptoms [9].

Vessels that may exhibit abnormal findings on F18-FDG PET-CT that would support the diagnosis of TKA are the thoracic aorta, abdominal aorta, branch arteries of the arch of aorta, and mesenteric, left or right carotid, left or right subclavian, and left or right renal arteries. Presence or absence of symmetrical involvement of the carotid, subclavian, or renal arteries should also be noted [5].

It has been found that one of the key values of PET-CT imaging of TKA is that it can detect LVV in patients who had been previously treated with immunosuppression [8, 10], a typical

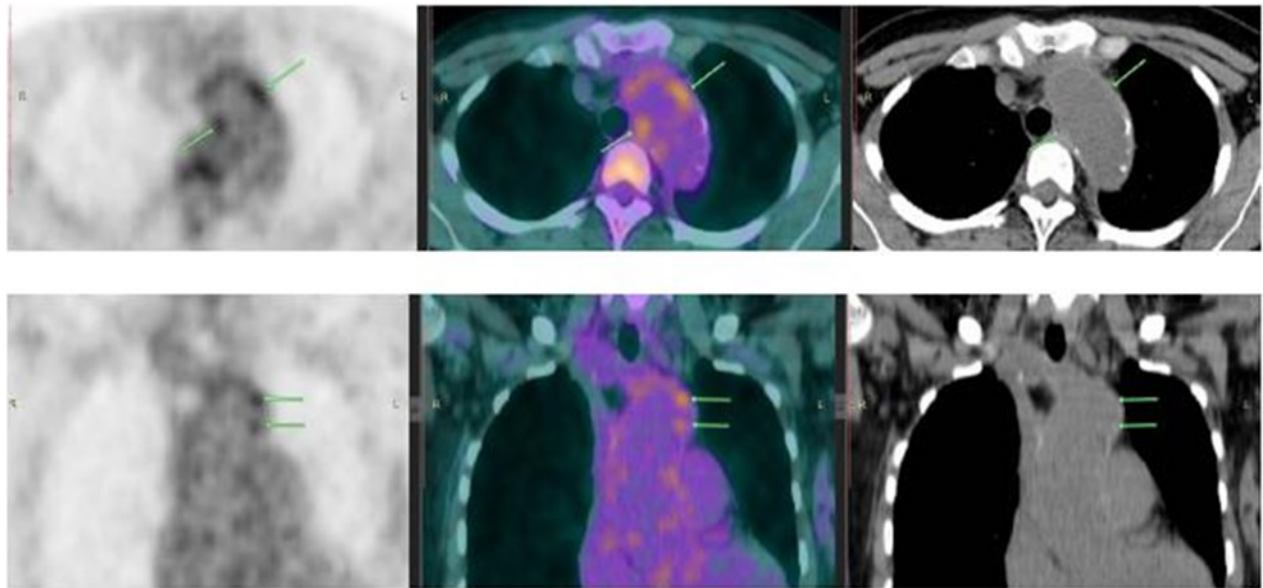


FIGURE 1. F18-FDG PET (leftmost column), PET-CT fused (middle column), and CT (rightmost column) images showing heterogenous radiotracer uptake in the arch of the aorta with associated enhancement (arrows).

treatment for the disease [1]. Thus, F18-FDG may provide valuable information regarding diseases status, recurrence evaluation, and response to treatment [11].

Morphologic findings that are typical of TKA are irregular vessel walls, stenosis, poststenotic dilation, aneurysm formation, occlusion, and evidence of increased collateral circulation [1]. In this patient, morphologic changes were observed such as dilatation of the ascending and aortic arch with distal gradual tapering in the latter. The descending aorta, however, was of normal caliber. These morphologic changes imply a prolonged chronicity of the disease.

Mild, heterogenous FDG uptake was noted along the walls of the arch of the aorta on PET with enhancement on CT, likely from TKA's characteristic inflammatory process. The intensity of F18-FDG uptake may be suggestive of TKA's relative activity at the time of imaging, though studies relating standard uptake value (SUV) and disease activity have been inconsistent so far [6]. However, a joint procedural recommendation of the European Association of Nuclear Medicine (EANM), the Society of Nuclear Medicine and Molecular Imaging (SNMMI), and the PET Interest Group (PIG), endorsed by the American Society of Nuclear Cardiology (ASNC) proposed the use of a standardized 0-to-3 grading system as follows: 0 = no uptake (\leq mediastinum); 1 = low-grade uptake ($<$ liver); 2 = intermediate-grade

uptake ($=$ liver), 3 = high-grade uptake ($>$ liver), with grade 2 possibly indicative and grade 3 considered positive for active LVV [12]. Following this grading system, this patient's uptake in the arch of the aorta would be considered grade 3, a high-grade uptake.

While it is unclear whether or not this patient may have been treated with immunosuppressants, such as corticosteroids, during her most recent hospital admission when TKA was diagnosed, she was not taking regular immunosuppressants at the time of this PET-CT imaging and F18-FDG did indeed get taken up by the walls of the arch of the aorta.

It is clear from various studies that F18-FDG PET-CT has value in providing information in helping diagnose TKA in its early and active disease processes before changes in morphology and vascular structure occur, information of advanced stages has been mainly provided by morphological imaging [13], as the expectation is that atherosclerosis would stifle FDG uptake.

However, this patient does have morphologic changes with a high level of FDG uptake in the arch of the aorta based on the proposed 0- to 3-grading system. Information regarding the utility of F18-FDG PET-CT in the continuing monitoring of SUV values with emphasis

on the correlation of any trend in change with morphologic progression of a patient diagnosed with TKA has been scarce in English literature and may be worth investigating in future studies.

SUMMARY

F18-FDG PET-CT imaging of a 24-year old female patient diagnosed with Takayasu's Arteritis was acquired which showed high-level heterogenous FDG uptake in the walls of the arch of the aorta with enhancement. This was observed in the presence of morphological changes such as dilatation of the ascending and aortic arch with distal gradual tapering in the latter and prominence of the right common carotid artery and the main pulmonary artery with gradual pruning of the latter. These findings suggest an advanced disease. In addition to F18-FDG PET-CT's current potential for early diagnosis and recurrence detection, future studies regarding the utility of SUV measurements in the continuing monitoring of advanced Takayasu's arteritis may be considered.

INFORMED CONSENT

Informed consent was obtained from the patient for the purpose of publishing this case report.

REFERENCES

1. Langford CA and Fauci AS. The Vasculitis Syndromes. In: Loscalzo J, Fauci AS, Kasper DL, Hauser SL, Longo DL, and Jameson JL, eds. *Harrison's Principles of Internal Medicine*. 21st ed. New York: McGraw Hill; 2022:363:2802-2817.
2. Mitchell RN and Halushka MK. Blood Vessels. In: Kumar V, Abbas AK, Aster JC, and Turner JR, eds. *Robbins & Coltran Pathologic Basis of Disease*. 10th ed. Philadelphia: Elsevier; 2021:11:485-525.
3. Alnabwani D, Patel P, Kata P, Patel V, Okere A, and Cheriya P. The Epidemiology and Clinical Manifestations of Takayasu Arteritis: A Descriptive Study of Case Reports. 2021 Sep 15. *Cureus*;13(9):e17998.
4. Muratore F, Pipitone N, Salvarani C, and Schmidt WA. Imaging of vasculitis: state of the art. *Best Pract Res Clin Rheumatol*. 2016 Aug;30(4):688-706.
5. Grayson PC, Ponte C, Suppiah R For the DCVAS Study Group, et al. 2022 American College of Rheumatology/ EULAR classification criteria for Takayasu arteritis. *Annals of the Rheumatic Diseases* 2022;81:1654-1660.
6. Zhang X, Zhou J, Sun Y, Shi H, Ji Z, and Jiang L.

- 18F-FDG-PET/CT: an accurate method to assess the activity of Takayasu's arteritis. *Clin Rheumatol*, 2018;37:1927-1935.
7. Meller J, Strutz F, Siefker U, et al. Early diagnosis and follow-up of aortitis with [18F]FDG PET and MRI. *Eur J Nucl Med Mol Imaging* 2003;30:730-736.
8. Shimol JB, Amital H, Lidar M, Domachevsky L, Shoenfeld Y, and Davidson T. The utility of PET/CT in large vessel vasculitis. *Sci Rep* 2020;10:17709.
9. Na C, Jin-bai H. 18F-FDG PET/CT in the diagnosis of Takayasu arteritis: A case report. *Radiology Case Reports* 2022;17:489-491.
10. Daisuke T, Go H, Takashi I, et al. Role of FDG PET-CT in Takayasu Arteritis: Sensitive Detection of Recurrences. *JACC: Cardiovascular Imaging* 2012;5(4):422-429.
11. Parihar A, Kumar R, Singh H, and Mittal B. 18F-FDG PET/CT in Takayasu Arteritis - Active or Inactive? *J Nucl Med* 2020;61(supplement 1):643.
12. Slart RHJA, Writing group, Reviewer Group, et al. FDG-PET/CT(A) imaging in large vessel vasculitis and polymyalgia rheumatica: joint procedural recommendation of the EANM, SNMMI, and the PET Interest Group (PIG), and endorsed by the ASNC. *Eur J Nucl Med Mol Imaging* 2018;45:1250-1269.
13. Ben-Haim S, Gaciovic S, and Israel O. Cardiovascular Infection and Inflammation. *Semin Nucl Med*. 2009;39:103-114.

A Comparative Study of Two Commercial Software Programs in Measuring Myocardial Left Ventricular Perfusion and Function among Filipino Patients undergoing Gated SPECT-MPI

Mary Amie Gelina E. Dumatol, MD, Jerry M. Obaldo, MD, MHA, Apolonio Alecksandr T. Molina, RMT, MSMT

Nuclear Medicine Division, Philippine Heart Center

E-mail address: medumatol@alum.up.edu.ph

ABSTRACT

Background:

Quantitative Perfusion SPECT / Quantitative Gated SPECT (QPS/QGS) and Corridor 4DM are among the most commonly used software for myocardial perfusion imaging (MPI). Studies involving the comparability of such programs remain limited, particularly for SPECT-CT cameras.

Methodology:

Adult patients who underwent dipyridamole gated SPECT-MPI using technetium-99m sestamibi were studied. Parameters of myocardial perfusion and left ventricular function, namely summed stress score (SSS), summed rest score (SRS), summed difference score (SDS), total stress defect extent (TDE), end systolic volume (EDV), and ejection fraction (EF), were derived using the QPS/QGS and 4DM software. Statistical analysis was performed to examine the differences between the two.

Results:

One-hundred thirteen (113) patients were included. There were statistically significant differences between QPS and 4DM in terms of uncorrected SSS (median difference = 2), SDS (median difference = 3), and TDE (median difference = 3) ($p < 0.001$); and attenuation-corrected SSS (median difference = 2) ($p < 0.001$), SRS (median difference = 1) ($p = 0.008$), SDS (median difference = 2) ($p < 0.001$), and TDE (median difference = 2) ($p = 0.029$). Likewise, statistically significant differences were seen between QGS and 4DM in terms of left ventricular EDV and EF ($p < 0.001$). Perfusion and ventricular function measures produced by 4DM tended to be higher than those of QPS/QGS.

Conclusion:

4DM-derived parameters of myocardial perfusion defects and left ventricular function in SPECT MPI were significantly higher than those derived through QPS/QGS. MPI software should not be used interchangeably in conducting follow-up imaging studies.

Keywords: myocardial perfusion imaging (MPI), technetium-99m sestamibi, dipyridamole, Cedars-Sinai Quantitative Perfusion SPECT / Quantitative Gated SPECT (QPS/QGS), Corridor 4DM, SPECT-CT

INTRODUCTION

Myocardial perfusion imaging (MPI) using single photon emission computed tomography (SPECT) is one of the most frequently utilized modalities in cardiac imaging, particularly in aiding the diagnosis and management of coronary artery disease (CAD) [1]. Clinical visual analysis remains the recommended method for interpretation of SPECT-MPI studies. However, technological advancements throughout the years have led to the development of software programs to enable automated quantification of such imaging studies, allowing an objective and more reproducible way of assessment.

MPI involves a number of measurements and grading parameters designed to quantify relative myocardial perfusion, ischemia, viability, and ventricular function [2]. Readings produced by these quantitative measures have been shown to be comparable with traditional visual analysis by physician interpreters in several independent studies, [3 - 5] but the applicability of such findings in other nuclear medicine centers may be influenced by differences brought about by the machine utilized, the imaging protocol followed, the population being studied, and the computer software program used in acquisition and processing [6]. Studies exploring the comparability of SPECT-MPI quantitative measures generated through the commercially available software programs, especially with regards to gated-derived parameters, such as left ventricular volumes and ejection fraction, remain scarce [7 - 9]. Even fewer have been done using data with attenuation correction, a technique that has become routine in the Philippine Heart Center MPI protocol to prevent certain artifacts on images.

Quantitative Perfusion SPECT / Quantitative Gated SPECT (QPS/QGS, Cedars-Sinai Medical Center, Los Angeles, California, USA) and Corridor4DM (4DM, University of Michigan, Ann Arbor, Michigan, USA) are among the most widely used commercially available software programs used globally in performing MPI. Both are able to provide information on myocardial perfusion through automated indices, such as summed stress score (SSS), summed rest score (SRS), summed difference score (SDS), and total stress defect extent (TDE). Assessment of left ventricular function is likewise achieved with automated parameters, including end diastolic and systolic volumes, and ejection fraction.

This study therefore aims to compare two software programs, namely Quantitative Perfusion SPECT / Quantitative Gated SPECT (QPS/QGS, Cedars-Sinai Medical Center, Los Angeles, California, USA) and Corridor 4DM (4DM, University of Michigan, Ann Arbor, Michigan, USA), in calculating perfusion and gated indices of SPECT-MPI. In doing so, it hopes to improve the degree of precision and accuracy by which SPECT-MPI studies are conducted, particularly in the Philippine setting.

METHODOLOGY

One-hundred thirteen (113) adult patients referred to the Philippine Heart Center Nuclear Medicine Division for dipyridamole pharmacologic stress using technetium-99m sestamibi SPECT-MPI from January 1, 2019 to December 31, 2020 were included in this retrospective cross-sectional study. Non-probability consecutive sampling was done. Exclusion criteria were as follows: incomplete clinical data, suboptimal scans, and undertaking of percutaneous coronary intervention (PCI) and/or coronary artery bypass graft (CABG) surgery. This study was granted approval by the Technical Review Committee and the Institutional Ethics Review Board of the Philippine Heart Center.

Image Acquisition

A one-day dipyridamole pharmacologic stress gated SPECT-MPI protocol using technetium-99m sestamibi was used in testing all patients included in this study. Patients discontinued beta blockers and calcium channel antagonists for 24-48 hours, refrained from consuming caffeine-containing food and beverages for 24 hours, and fasted for 4 hours prior to the procedure.

Resting dose of technetium-99m sestamibi (8 mCi / 296 MBq) was given intravenously and allowed to distribute optimally. Rest imaging was done after 45 minutes with the patient positioned supine using a dual-head hybrid SPECT/CT machine (Discovery NM/CT 670 ES, GE Healthcare) equipped with a low-energy high resolution (LEHR) collimator. A step-and-shoot acquisition type was followed, with camera detectors configured at 90 degrees. Thirty-two projections were obtained over a 180-degree orbit (45 degrees right anterior oblique to 45 degrees left posterior oblique). Symmetric energy windows of 20% were used over the 140 keV photopeaks, while ECG gating was set at a 40% R-R

window. Attenuation correction was applied using low-dose CT.

Baseline electrocardiograph (ECG), blood pressure (BP), and heart rate (HR) were recorded prior to administration of pharmacologic stress. Dipyridamole (0.56 mg/kg) was infused over 4 minutes with continuous monitoring of the ECG, BP, and HR over the next 15 minutes. Stress dose of technetium-99m sestamibi (24 mCi / 888 MBq) was administered and allowed to distribute optimally. Stress imaging was done after 30 minutes using the same machine and imaging parameters as with rest imaging.

Image Processing

Processing of acquired images and data was done through the GE Xeleris workstation (version 4.0) using the QPS/QGS and 4DM software programs by an experienced nuclear medicine technologist, with minimal manual intervention to avoid bias and variability. Using both QPS/QGS and 4DM, fully automated parameters of perfusion and left ventricular function were generated, namely SSS, SRS, SDS, TDE, left ventricular volumes, and ejection fraction, both for the uncorrected and attenuation corrected images.

Sample Size Calculation

Based on the 64.17% total concordance of 4DM and QPS/QGS, [9] 5% level of significance, and 10% desired half-width of the confidence interval, a minimum of 89 patients was required for this study [10].

Statistical Analysis

Descriptive statistics was used to summarize the demographic and clinical characteristics of the patients. Frequency and proportion were used for categorical variables, median, and inter quartile range for non-normally distributed continuous variables, and mean and SD for normally distributed continuous variables. Wilcoxon Signed rank test was used to determine the difference between QPS/QGS and 4DM automated quantitative perfusion results and automated quantitative gated results. All statistical tests were two tailed tests. Shapiro-Wilk test was used to test the normality of the continuous variables. Missing values were neither replaced nor estimated. Null hypotheses were rejected at 0.05 α -level of significance. STATA 13.1 was used for data analysis.

RESULTS

One-hundred thirteen (113) patients were included in the final study, the baseline characteristics of whom are summarized in Table 1.

Automated Quantitative Perfusion Results

Statistically significant differences were seen between the summed rest scores (SRS) (median difference = 2), summed difference scores (SDS) (median difference = 3), and total stress deficit extent (TDE) (median difference = 3) values generated by the QPS and 4DM software for the non-corrected images ($p < 0.001$). The measured summed stress scores (SSS) for both software showed good concordance with no statistically significant difference (median difference = 2; $p = 0.891$). Of note, non-corrected images analyzed using the 4DM software produced more SDS measures less than 0. The extent of defects calculated was observed to be larger using 4DM, compared to QPS (Table 2).

For the attenuation corrected images, statistically significant differences were observed between the QPS and 4DM-generated perfusion values of SSS (median difference = 2), SRS (median difference = 1), SDS (median difference = 2), and TDE (median difference = 2). As was seen in the analysis of NC images, the 4DM software still produced more SDS measures less than 0, compared with the QPS software (Table 2).

Automated Quantitative Gated Results

Statistically significant differences were seen between the left ventricular end diastolic volumes (EDV) and ejection fractions (EF) calculated by the QGS and the 4DM software for both stress and rest data sets. Higher EDV and EF values were generated by the 4DM software, compared with the QGS software. On the contrary, the left ventricular end systolic volumes (ESV) generated by the 2 software showed no significant differences for both stress and rest data sets (Table 3).

DISCUSSION

This study compared automated SPECT-MPI parameters of myocardial perfusion and left ventricular function derived from two commercially available software

TABLE 1. Patient population baseline characteristics
(N = 113)

Characteristic	Frequency (%) / Mean ± SD
Age, years	59.88 ± 14.24
Sex (Male / Female)	63 (55%) / 50 (44%)
Height, cm	161.06 ± 9.46
Weight, kg	68.46 ± 14.96
Past medical history	
Hypertension	88 (78%)
Dyslipidemia	61 (54%)
Diabetes mellitus	34 (30%)
Past myocardial infarction	21 (19%)
Chronic kidney disease	12 (11%)
Cerebrovascular disease	10 (9%)
Smoking History	
Smoker	30 (27%)
Non-smoker	83 (73%)
Symptomatology Chest Pain	
None	48 (42%)
Nonspecific chest pain	17 (15%)
Atypical chest pain	29 (26%)
Typical chest pain	19 (17%)
Exertional dyspnea	64 (57%)
Easy fatigability	62 (55%)
Orthopnea	13 (12%)

TABLE 2. QPS/QGS and 4DM automated
quantitative perfusion results

	QPS/QGS	4DM	Difference	p-value
	Median (IQR)			
NON-CORRECTED (NC) IMAGES				
SSS	3 (1 to 8)	3 (1 to 6)	2 (1 to 4)	0.891
SRS	1 (0 to 4)	3 (1 to 8)	2 (1 to 4)	< 0.001
SDS	1 (0 to 3)	0 (-2 to 2)	3 (1 to 5)	< 0.001
TDE	4 (1 to 9)	4 (0 to 12)	3 (2 to 8)	< 0.001
ATTENUATION-CORRECTED (AC) IMAGES				
SSS	3 (0 to 8)	1 (0 to 6)	2 (1 to 4)	< 0.001
SRS	0 (0 to 3)	1 (0 to 5)	1 (0 to 2)	0.008
SDS	2 (0 to 4)	0 (-1 to 1)	2 (1 to 5)	< 0.001
TDE	3 (0 to 8)	0 (0 to 7)	2 (0 to 6)	0.029

TABLE 3. QPS/QGS and 4DM automated quantitative gated results

	QPS/QGS	4DM	Difference	p-value for difference
	Median (IQR)			
STRESS				
LV EDV	92 (65 to 134)	104 (72 to 140)	9 (5 to 16)	< 0.001
LV ESV	35 (22 to 68)	36 (21 to 68)	4 (2 to 9)	0.329
EF	60 (42 to 68)	66 (46 to 73)	4 (1 to 8)	< 0.001
REST				
LV EDV	84 (62 to 129)	94 (69 to 145)	9 (6 to 17)	< 0.001
LV ESV	34 (20 to 71)	32 (21 to 67)	4 (2 to 8)	0.522
EF	59 (44 to 68)	65 (49 to 73)	5 (2 to 9)	< 0.001

programs, namely QPS/QGS and 4DM. Only the SSS values derived from the NC images as well as the stress and rest ESV measures were comparable between the 2 software. Statistically significant differences were observed between measurements of SSS, SDS, and TDE for the NC images; all perfusion elements from the AC images; and the derived left ventricular EDV and EF values for both software programs.

Automated parameters of myocardial left ventricular perfusion and function, including LV volumes and ejection fraction, can be easily derived through the software programs used in conducting SPECT-MPI procedures [2]. These measurements enable a more objective and precise interpretation of such imaging studies, potentially addressing the inherent constraints possessed by visual readings conducted by physicians that rely heavily on individual opinion and experience.

Our results concur with past studies conducted in other countries that demonstrated considerable differences between automated parameters of perfusion and left ventricular function generated by different cardiac software [7 - 9] using data acquired without application of attenuation correction. Additionally, our study compared perfusion and function measures generated by QPS/QGS and 4DM using attenuated corrected data and likewise found significant differences between the two sets of measures. It has become routine to use attenuation correction through low-dose CT at our institution, given its role in addressing the pitfalls of apparent defects caused by soft-tissue attenuation and improving the diagnostic accuracy of MPI studies [11]. Our institution makes use of both the non-corrected (NC) and attenuated-corrected (AC) images for optimal interpretation of MPI studies.

Quantification of perfusion using MPI software entails the mapping of derived counts from each patient's extracted perfusion distribution data [2]. This relative distribution is then compared to a normal perfusion database, which has been generated using perfusion data from patients with low pretest likelihood of coronary artery disease, in order to generate myocardial perfusion scores. These constructed databases are matched for sex, radiopharmaceutical used, and position during imaging. It should be noted that the analyses in this study made use of the manufacturer-provided normal databases that were derived from a North American population. Custom normal databases can be

made and used in place of the default databases that come with the software. The studies conducted by Wolak et al. [12] and Guner et al. [13] showed no significant difference between the QPS/QGS and 4DM automated parameters generated using either the manufacturer-provided or their institution-based databases. On the contrary, studies done in other territories, including Japan [14], Iran [15], and Spain [16], have demonstrated significant differences with the perfusion parameters generated using their population-specific databases and the manufacturer-provided ones, differences that may be attributed to differences in body habitus of the said populations. It is possible that the studies that showed no significant differences may have involved patient populations with similar builds as the patients included in the construction of the default databases. At the time of writing, the Philippines has yet to produce a population-based normal database of its own, and the effect of such a database when applied to automated analysis using MPI software remains to be seen.

Apart from the normal databases applied, another factor that may have influenced the differences observed between the parameters generated by the two software is variation in method of segmentation, limit determination, and polar map generation by which the two programs handle perfusion and gated data [17 - 20]. For instance, in determining myocardial perfusion boundaries, 4DM proceeds with segmentation by first identifying LV center and axial limits, then doing boundary detection through the use of long-axis slices. On the other hand, QPS uses an iterative approach in automatic segmentation, followed by boundary extraction using short-axis slices. Limit determination is also influenced by the different models used as basis for valve plane estimation, wherein 4DM models work under the assumption that basal limits are alike in the septal and lateral myocardial walls, while QPS models presumes that the septal wall is shorter, thereby leading to different estimations on each LV side. Polar map generation is likewise different between the two programs, particularly in data sampling for the apical segments, in which 4DM maps using cylindrical sampling while QPS samples using a spherical map.

In the analysis for automated myocardial perfusion, we observed that the 4DM software tended to produce SDS measures less than 0. This is suggestive of a reverse perfusion pattern, which denotes defects that appear or apparently worsen during rest imaging with respect to

stress imaging. When observed in myocardial perfusion imaging using technetium-99m sestamibi, the implications of this phenomenon remain widely uncertain, though certain studies have shown association of the pattern with subendocardial scarring, chronic coronary artery disease, and previous history of myocardial infarction [21 - 22]. However, reverse perfusion patterns are more often than not artifactual in nature, resulting from various causes including but not limited to soft-tissue attenuation and erroneous normalization during processing [23]. The 4DM software was found to less likely adjust derived perfusion parameters with respect to these artifacts as compared to the QPS program, though it should be noted that automated analysis using MPI software are, in general terms, unable to fully account for such as compared to visual analysis by expert readers.

ECG-gated SPECT allows evaluation of left ventricular function alongside myocardial perfusion assessment. Past studies have shown good association between LV volumes and ejection fractions derived by 4DM and QGS [17, 24 - 25], though the study by Ather et al. [9] was able to demonstrate significant differences between such parameters of LV function. Our study results likewise revealed statistically significant differences between the EDV and EF generated by the two cardiac software, but not the ESV. As with perfusion imaging, the software programs do differ in the methods and algorithms used in calculation of values.

Our study possesses a number of limitations. Only direct comparison of the automated perfusion defects and LV function parameters derived from the two software programs was done, with no gold standard used. Manufacturer-provided databases were used for both the 4DM and QPS/QGS software, with the one used for the former different from that used for the latter. Thus, there may be variations in subject composition and data sets used to construct the databases, and the values derived may be influenced. This study was unable to account for these factors.

At present, no single MPI software program can be considered more 'correct' over the others. This is due to the lack of consensus over which modality should be used as the gold standard, and thus the basis for comparison. The University of Michigan's Corridor 4DM and the Cedars-Sinai Cardiac Suite QPS/QGS software are among the most commonly utilized programs in doing

SPECT MPI, and both programs have been individually validated for use and application. However, the significant differences observed between the parameters of perfusion and LV function derived using the two software make it essential for institutions to use the same program for monitoring and follow-up studies.

CONCLUSION

There are statistically significant differences between QPS/QGS and 4DM parameters of myocardial perfusion and left ventricular function in SPECT MPI, with defects and values derived through 4DM tending to be higher than those of QPS/QGS. MPI software should not be used interchangeably in conducting follow-up imaging studies.

REFERENCES

1. Abbott B, Case J, Dorbala S, Einstein A, Galt J, Pagnanelli R et al. Contemporary Cardiac SPECT Imaging—Innovations and Best Practices: An Information Statement from the American Society of Nuclear Cardiology. *Circulation : Cardiovascular Imaging*. 2018;11(9).
2. Garcia, E., Slomka, P., Moody, J., Germano, G. and Ficaro, E., 2019. Quantitative Clinical Nuclear Cardiology, Part 1: Established Applications. *Journal of Nuclear Medicine*, 60 (11), pp.1507-1516.
3. Leslie W, Tully S, Yogendran M, Ward L, Nour K, Metge C. Automated quantification of 99mTc sestamibi myocardial perfusion compared with visual analysis. *Nuclear Medicine Communications*. 2004;25(8):833-838.
4. Arsanjani R, Xu Y, Hayes S, Fish M, Lemley M, Gerlach J et al. Comparison of Fully Automated Computer Analysis and Visual Scoring for Detection of Coronary Artery Disease from Myocardial Perfusion SPECT in a Large Population. *Journal of Nuclear Medicine*. 2013;54(2):221-228.
5. Driessen R, Raijmakers P, Danad I, Stuijzand W, Schumacher S, Leipsic J et al. Automated SPECT analysis compared with expert visual scoring for the detection of FFR-defined coronary artery disease. *European Journal of Nuclear Medicine and Molecular Imaging*. 2018;45 (7):1091-1100.
6. Rubeaux M, Xu Y, Germano G, Berman D, Slomka P. Normal Databases for the Relative Quantification of Myocardial Perfusion. *Current Cardiovascular Imaging Reports*. 2016;9(8).
7. Knollmann D, Knebel I, Koch K, Gebhard M, Krohn T, Buell U et al. Comparison of SSS and SRS calculated from normal databases provided by QPS and 4D-M SPECT manufacturers and from identical institutional normals. *European Journal of Nuclear Medicine and Molecular Imaging*. 2007;35(2):311-318.

8. Alexiou S, Georgoulas P, Angelidis G, Valotassiou V, Tsougos I, Psimadas D, et al. Myocardial perfusion and left ventricular quantitative parameters obtained using gated myocardial SPECT: Comparison of three software packages. *Journal of Nuclear Cardiology*. 2016;25(3):911–24.
9. Ather, S., Iqbal, F., Gulotta, J., Aljaroudi, W., Heo, J., Iskandrian, A. and Hage, F., 2014. Comparison of three commercially available softwares for measuring left ventricular perfusion and function by gated SPECT myocardial perfusion imaging. *Journal of Nuclear Cardiology*, 21(4), pp.673-681.
10. Peacock JL, Peacock PJ. Research design. (ed). Oxford handbook of Medical Statistics. United States: Oxford University Press; 2011. pp. 60-61.
11. Huang J-Y, Huang C-K, Yen R-F, Chien K-L, Wu Y-W. Diagnostic effect of attenuation correction in myocardial perfusion imaging in different coronary arteries: A systematic review and meta-analysis. *Frontiers in Cardiovascular Medicine*. 2021;8.
12. Wolak A, Slomka PJ, Fish MB, Lorenzo S, Acampa W, Berman DS, et al. Quantitative myocardial-perfusion SPECT: Comparison of three state-of-the-art software packages. *Journal of Nuclear Cardiology*. 2007Oct20;15(1):27–34.
13. Guner LA, Karabacak NI, Cakir T, Akdemir OU, Kocaman SA, Cengel A, et al. Comparison of diagnostic performances of three different software packages in detecting coronary artery disease. *European Journal of Nuclear Medicine and Molecular Imaging*. 2010;37(11):2070–8.
14. Nakajima K, Okuda K, Kawano M, Matsuo S, Slomka P, Germano G, et al. The importance of population-specific normal database for quantification of myocardial ischemia: Comparison between Japanese 360 and 180-degree databases and a US database. *Journal of Nuclear Cardiology*. 2009;16(3):422–30.
15. Hosseini, A., Fattahi, M. R., Mehrpooya, M., Khosravi, A., Farzanefar, S., Abbasi, M. Normal perfusion and function myocardial perfusion imaging indices in Iranian normal females. *Iranian Journal of Nuclear Medicine*, 2023; 31(1): 29-34. doi: 10.22034/irjnm.2022.40036.
16. Cuberas-Borrós G, Aguadé-Bruix S, Boronat-de Ferrater M, Muxí-Pradas MÁ, Romero-Farina G, Castell-Conesa J, et al. Normal myocardial perfusion SPECT database for the Spanish population. *Revista Española de Cardiología (English Edition)*. 2010Aug;63(8):934–42.
17. Lin GS, Hines HH, Grant G, Taylor K, Ryals C. Automated Quantification of Myocardial Ischemia and Wall Motion Defects by Use of Cardiac SPECT Polar Mapping and 4-Dimensional Surface Rendering. *Journal of Nuclear Medicine Technology*. 2006Mar;34(1):3–17.
18. Schaefer WM, Lipke CSA, Standke D, Kühl HP, Nowak B, Kaiser H-J, et al. Quantification of Left Ventricular Volumes and Ejection Fraction from Gated 99mTc-MIBI SPECT: MRI Validation and Comparison of the Emory Cardiac Tool Box with QGS and 4D-MSPECT. *Journal of Nuclear Medicine*. 2005Aug;46(8):1256–63.
19. Germano G, Kavanagh PB, Slomka PJ, Van Kriekinge SD, Pollard G, Berman DS. Quantitation in gated perfusion SPECT imaging: The Cedars-Sinai approach. *Journal of Nuclear Cardiology*. 2007;14(4):433–54.
20. Ficaro EP, Lee BC, Kritzman JN, Corbett JR. Corridor4DM: the Michigan Method for Quantitative Nuclear Cardiology. *Journal of Nuclear Cardiology*. 2007;14(4):455–65.
21. Araujo W. Artifactual reverse distribution pattern in myocardial perfusion spect with technetium-99m Sestamibi. *Journal of Nuclear Cardiology*. 2000;7(6):633–8.
22. Fallahi B, Beiki D, Salehi Y, Emami-Ardekani A, Fard-Esfahani A, Aghahosseini F, et al. Reverse perfusion pattern in myocardial perfusion imaging using technetium -99m-sestamibi in patients with intermediate risk for coronary artery disease in relation to the time of acquisition and intensity of visceral uptake as artifactual causes. *Nuclear Medicine Communications*. 2017;38(1):15 – 20.
23. Schillaci O, Tavolozza M, Di Biagio D, Lacanfora A, Chiaravalloti A, Palombo E, Catalano R, Simonetti G. Reverse perfusion pattern in myocardial spect with 99mTc - sestaMIBI. *Journal of Medicine and Life*. 2013;6(3):349-54.
24. Nakajima K, Higuchi T, Taki J, Kawano M, Tonami N. Accuracy of ventricular volume and ejection fraction measured by gated myocardial SPECT: comparison of 4 software programs. *Journal of Nuclear Medicine*. 2001;42(10):1571-8.
25. Calandri E, Guana F, Pultrone M, Leuzzi S, Chiorino G, Soligo E, et al. Evaluation of left ventricular volumes and ejection fraction from gated myocardial perfusion SPECT processed with “Myovation evolution”: Comparison of three automated software packages using Cardiac Magnetic Resonance as reference. *Current Radiopharmaceuticals*. 2021;14(2):112–20.

ACKNOWLEDGEMENTS

The authors would like to thank Mr. Rhalp Jaylord Valenzuela for his valuable statistical inputs, and the staff members of the Philippine Heart Center Nuclear Medicine Division for the assistance and support that lead to the completion of this research project.



PSNM 40TH ANNUAL CONVENTION

Philippine Society of Nuclear Medicine



INNOVATE ADVANCE SCINTILLATE

8 - 9 February 2025

Fiesta Pavilion

The Manila Hotel



Unlock High Quality Compounding with Esco's innovative solutions today!



Isoclean® Healthcare Platform Isolator
[HPI-2G (w/ filter below) and HPI-4N/4P (w/o filter below)]



Streamline® Compounding Isolator (SCI-2G)



Cytoculture® Cytotoxic Safety Cabinet (CYT-4A)



Labculture® Class II Type B2 Biosafety Cabinet (LB2-)



Infinity® Pass Box / Cleanroom Transfer Hatch (EPB-A and EPB-S)



Dynamic Pass Box (DPB-S606060) and Static Pass Box (SPB-S606060)



HP Series Lab Refrigerator (HR1-700S and HR1-1500S)

ESCO
LIFESCIENCES GROUP



@escophilippines



@escophilippines



@EscoLifesciencesGroup
@EscoPharma



@escophilippines

ESCO PHILIPPINES INC.

Unit 707E, 7th Floor, East Tower Four E-Com Center
Block 22, Seaside Cor Diokno Ave. MOA Complex,
Pasay City 1300

+63 (02) 8478 0384 / 0917 806 8026

philippines@escolifesciences.com

www.escolifesciences.com
www.esco-pharma.com

**Symbia Pro.specta SPECT/CT
with myExam Companion**

Modernize to MAXIMIZE



Take your nuclear medicine department into the future with intelligent SPECT/CT imaging. Symbia Pro.specta™ with myExam Companion™ gives you the power of more.

Redefine performance with new standards for SPECT/CT

Automatic SPECT motion correction and up to 64-slice CT enable faster scanning at the highest image quality.¹

Reach your full potential with a smart workflow

A single, intuitive interface automates steps across the entire workflow—helping you achieve high-quality, reproducible results.

Achieve optimized imaging from dedicated clinical tools

A multi-purpose SPECT/CT that transforms into a specialized camera for cardiology, neurology, oncology, theranostics, and more.

¹ Based on competitive literature at time of publication. Data on file.

Symbia Pro.specta SPECT/CT is not commercially available in all countries. Future availability cannot be guaranteed. Please contact your local Siemens Healthcare organization for further details.

Learn more at siemens-healthineers.com/symbia-prospecta

SIEMENS
Healthineers